

A Low-Complexity Architecture for Multi-access Coded Caching Systems with Arbitrary User-cache Access Topology

Ting Yang, Kai Wan, *Member, IEEE*, Minquan Cheng, *Member, IEEE*,
 Xinping Yi, *Member, IEEE*, Robert Caiming Qiu, *Fellow, IEEE*,
 and Giuseppe Caire, *Fellow, IEEE*

Abstract

This paper studies the multi-access coded caching (MACC) problem under arbitrary user-cache access topology, which extends existing MACC models that rely on highly structured and combinatorially designed topology. We consider an MACC system consisting of a single server, Λ cache nodes, and K user nodes. The server stores N equal-size files, each cache node has a storage capacity of M files, and each user can access an arbitrary subset of cache nodes and retrieve the cached content stored in those caches. The objective is to design a general and low-complexity delivery scheme under fixed cache-node placement for arbitrary access topology. We propose a universal graph-based framework for modeling the MACC delivery problem. In this framework, decoding conflicts among the requested packets are captured by a conflict graph, and design of the delivery is reduced to a graph coloring problem, where achieving a lower transmission load corresponds to coloring the graph using fewer colors. Under this formulation, the classical greedy coloring algorithm DSatur achieves a transmission load close to the index-coding (IC) converse bound, thereby providing a tight and practical benchmark. However, its computational complexity becomes prohibitive for large-scale graphs. To overcome this limitation, we

T. Yang, K. Wan, and R. C. Qiu are with the School of Electronic Information and Communications, Huazhong University of Science and Technology, 430074 Wuhan, China, (e-mail: {yangting, kai_wan, caiming}@hust.edu.cn).

M. Cheng is with the Key Laboratory of Education Blockchain and Intelligent Technology, Ministry of Education, and Guangxi Key Laboratory of Multi-Source Information Mining and Security, Guangxi Normal University, 541004 Guilin, China (e-mail: chengqinshi@hotmail.com).

X. Yi is with the Southeast University, Nanjing 210096, China, (e-mail: xyi@seu.edu.cn).

G. Caire is with the Electrical Engineering and Computer Science Department, Technische Universität Berlin, 10587 Berlin, Germany (e-mail: caire@tu-berlin.de).

develop a learning-based framework using graph neural networks (GNNs) that efficiently constructs near-optimal coded multicast transmissions and generalizes across diverse access topology and varying numbers of user nodes. In addition, we extend the IC converse bound for uncoded cache placement to MACC systems with arbitrary access topology and propose a low-complexity greedy approximation that closely matches the IC converse. Numerical results demonstrate that the proposed GNN-based scheme achieves transmission loads close to those of DSatur and the IC converse while significantly reducing computational time, making it suitable for large-scale MACC systems.

Index Terms

Multi-access coded caching (MACC), arbitrary access topology, Graph coloring, Graph Neural Networks (GNNs).

I. INTRODUCTION

The rapid proliferation of wireless devices and the growing demand for high-quality multimedia services have imposed significant pressure on modern wireless networks. User traffic is highly time-varying, leading to severe congestion during peak hours and underutilization of network resources during off-peak periods. Caching has been widely recognized as an effective approach to mitigate this imbalance by proactively storing popular content during off-peak times, thereby reducing redundant transmissions and alleviating peak-time traffic loads [1]. Coded caching was first introduced by Maddah-Ali and Niesen (MN) in [2]. In the MN coded caching model, a single server with a library of N files is connected to K users over a shared-link, where each user is equipped with a local cache of size M files. The system operates in two phases. In the *placement phase*, each user caches some packets of the files without knowledge of future demands. In the *delivery phase*, each user requests one file from the library, and the server broadcasts coded multicast transmissions to satisfy all users' demands. By jointly designing the placement and delivery phases, the MN scheme enables each multicast transmission to simultaneously serve multiple users, thereby creating a global caching gain. Specifically, when the cache size satisfies $M = \frac{tN}{K}$ for some $t \in \{0, 1, \dots, K\}$, the MN scheme achieves a worst-case normalized delivery load given by $\frac{K(1 - \frac{M}{N})}{1 + \frac{KM}{N}}$. Here, the term $1 - \frac{M}{N}$ corresponds to the *local caching gain*, representing the fraction of each file not stored in a user's cache, while the term $1 + \frac{KM}{N}$ captures the *coded caching gain*, which quantifies the average number of users simultaneously served by each multicast transmission. For general cache sizes, the achievable memory–load tradeoff can be

obtained via memory sharing. Moreover, when $N \geq K$, the MN scheme is order-optimal within a factor of 2 [2], and it is exactly optimal under the constraint of uncoded cache placement [3].

Despite its fundamental optimality, the MN coded caching scheme suffers from several practical limitations. First, the required subpacketization level, defined as the number of packets per file, grows exponentially with the number of users K . While information-theoretic achievability and converse results are typically established under the assumption of arbitrarily large file sizes, so that subpacketization does not pose a theoretical limitation, but in practical systems with finite file sizes, designing coded caching schemes with low subpacketization is of critical importance. To address this issue, the authors in [4] introduced a combinatorial framework known as the *placement delivery array* (PDA), which provides a universal characterization of coded caching schemes with uncoded cache placement and clique-cover-based delivery. Building on the PDA framework, a variety of coded caching schemes have been proposed [4]–[8] that significantly reduce the subpacketization level compared to the MN scheme. Second, the MN model relies on a highly idealized network topology, in which each user is equipped with a dedicated cache and is connected to the server through a single shared-link. The PDA framework naturally extends beyond this canonical setting and enables the systematic design of coded caching schemes for a wide range of more general network topology. These include combinatorial networks [9], device-to-device (D2D) networks [10], hierarchical caching networks [11], multi-antenna networks [12]–[17], as well as multi-access caching systems [18]–[21].

A. Multi-access coded caching

The classical coded caching framework assumes that each user is equipped with a dedicated cache that cannot be accessed by other users. In practical wireless and edge networks, however, caching resources are typically deployed at the network edge, such as base stations, access points, or edge servers. These edge caches often have larger storage capacities and can be accessed by multiple nearby users at high data rates, which naturally motivates the study of multi-access coded caching (MACC) problem. The MACC model was first introduced in [22], where cache nodes store content and cache-less users retrieve their requested data by accessing a subset of cache nodes according to a given user-cache access topology. Compared with the classical model where each user is equipped with a dedicated cache, MACC offers greater flexibility in cache deployment and enables higher spatial reuse of cached content.

Most existing works on MACC focus on highly structured and regular access topology, typically derived from specific combinatorial constructions. Such structures often impose rigid constraints on the numbers of user nodes and cache nodes, thereby limiting their applicability to more general and irregular network scenarios. A representative example is the cyclic wrap-around topology studied in [18], [19], [22], [23], where the numbers of users and cache nodes are identical and each user accesses a fixed number of neighboring cache nodes in a cyclic fashion. However, under practical cache size constraints, the achievable coded caching gain of such cyclic MACC topology is fundamentally limited. To overcome these limitations, several works have proposed MACC schemes based on more general combinatorial structures. In particular, symmetric combinatorial MACC topology with Λ cache nodes and $\binom{\Lambda}{a}$ users, where each user accesses exactly a cache nodes, were investigated in [24], [25]. Furthermore, cross-resolvable combinatorial designs were considered in [26]–[28], which construct MACC access topology with $\Lambda = mq$ cache nodes and $K = \binom{m}{a}q^a$ users, where $q = \frac{N}{M} \geq 2$ and $m \geq a$ are positive integers. More recently, a universal coded caching framework based on t -designs and t -group divisible designs (t -GDDs) was proposed in [29]. This framework subsumes cross-resolvable designs as special cases and enables the construction of coded caching schemes over a broader class of structured MACC topology.

B. Related Work

Existing learning-based caching techniques primarily aim to address practical scenarios in which content popularity is unknown and varies over time, and are predominantly based on reinforcement learning (RL) or deep reinforcement learning (DRL). Several works [30]–[32] estimate content popularity online to dynamically replace cached content such that the caching proportions of different files across network nodes are optimized. These methods typically adopt coded placement strategies such as Maximum Distance Separable (MDS) coding. However, they mainly focus on the cache placement phase and do not explicitly design or optimize the coded multicast transmissions in the delivery phase. Further studies also consider cooperative caching, content sharing, or scheduling among multiple base stations. Some works [33], [34] employ fractional caching by optimizing the proportions of each file cached across different nodes, while another work [35] considers file-level caching decisions, determining whether each entire file should be cached. By jointly optimizing cache placement, inter-base-station content sharing, and content acquisition costs, these approaches improve cache hit rates and reduce overall network

costs. Nevertheless, they similarly do not address the explicit construction of coded multicast transmissions in coded caching systems.

The work [36] combines learning mechanisms with coded caching in dynamic network environments to jointly optimize placement and delivery strategies. In such approach, RL is used to make high-level decisions, such as strategy selection or scheduling, while the underlying coded caching mechanisms are treated as fixed. As a result, the detailed construction of coded caching structures, including file subpacketization, cache placement patterns, and multicast transmission design in the delivery phase, is not explicitly optimized. Another research [37] applies reinforcement learning directly to the delivery phase, with the objective of learning efficient coded transmission strategies under a given cache placement. In this setting, the cache placement is assumed to be known and arbitrary at the bit level, and the RL determines how XOR combinations are formed. However, the resulting multicast coding decisions are typically learned in an unstructured manner, without explicitly exploiting the combinatorial structures.

RL-based approaches, such as [38], are not well suited to this setting, as they typically rely on repeated interactions with a fixed environment. In contrast, the MACC delivery problem involves dynamically varying conflict graphs induced by different user demands and access topology, which significantly limits the generalization capability of environment-specific RL policies and leads to high training complexity. By contrast, the proposed graph-based formulation enables learning models to operate directly on graph instances, allowing a single graph neural network (GNN) to generalize across heterogeneous access topology and user demand realizations without environment-specific retraining.

C. Motivations

Constructing efficient coded caching schemes for general and arbitrary user-cache access topology remains a challenging problem. Most existing works on multi-access coded caching (MACC) rely on highly structured access patterns and combinatorial designs, which do not readily extend to irregular or heterogeneous topology [24]–[29]. As a result, there currently exists no general and scalable framework for constructing near-optimal MACC schemes under arbitrary access topology. From a system design perspective, jointly optimizing cache placement and delivery under arbitrary user-cache access topology leads to a highly complex and topology-dependent combinatorial optimization problem. In MACC systems with structured access topology, cache placement schemes exploit strong symmetry and regularity in the topology, enabling compact

and elegant combinatorial constructions. However, such symmetry is generally absent in arbitrary and irregular access patterns, and even small changes in the access topology may invalidate a carefully designed placement scheme.

D. Contributions

This paper investigates the MACC problem under arbitrary user-cache access topology. By reformulating the MACC delivery problem within a universal graph-based framework, we develop efficient delivery schemes and practical performance benchmarks for large-scale and irregular MACC systems. The main contributions of this work are summarized as follows.

- We propose a universal graph-based formulation for the MACC delivery problem with arbitrary user–cache access topology. Under this formulation, decoding conflicts among requested packets induce a conflict graph, and the coded multicast delivery problem is reduced to a graph coloring problem, where each color corresponds to a multicast transmission.
- Based on the conflict graph formulation, we first apply the classical DSatur greedy graph coloring algorithm to construct coded multicast transmissions. We show that DSatur achieves delivery loads close to the IC converse bound, thereby serving as a strong and practical benchmark. Motivated by its performance but high computational complexity, we further develop a scalable learning-based graph coloring framework using GNNs, which achieves delivery loads close to the IC converse with significantly lower computational complexity than DSatur.
- We extend the index-coding converse bound for uncoded cache placement in [3] to MACC systems with arbitrary access topology. To overcome the prohibitive complexity of converse evaluation in large-scale MACC systems, we further propose a low-complexity greedy approximation that closely matches the IC converse bound.
- Experimental results validate the effectiveness of the proposed framework. Specifically, the DSatur algorithm achieves delivery loads that are very close to the IC converse bound, with a maximum gap no larger than 1.2%. Building on this benchmark, the proposed GNN-based approach achieves delivery loads within about 10% of DSatur, while reducing the runtime by a factor of 3 to 20 as the number of user nodes increases. Compared with a GIN-based learning approach, the proposed GNN reduces the number of required colors by approximately 20%-80% and achieves a runtime reduction of roughly one to two orders of magnitude. In addition, the proposed greedy converse closely approximates the IC converse,

achieving more than 97% of the bound while requiring only 10^{-2} to 10^{-6} of the computation time as the number of user nodes grows.

E. Paper Organization

The rest of this paper is organized as follows. Section II reviews the classical shared-link coded caching model and introduces the MACC system model with arbitrary user-cache access topology. It also presents a graph-based formulation that transforms the MACC delivery problem into a graph coloring problem. Section III provides the necessary preliminaries, including classical graph coloring and GNN-based graph coloring approaches, and the IC converse bound. Section IV introduces the proposed AI-aided delivery framework for MACC systems based on the conflict graph and GNN-based graph coloring. Section V presents a low-complexity greedy approximation of the IC converse bound. Simulation results and performance evaluations are provided in Section VI. Finally, Section VII concludes the paper.

F. Notations

The following notations are used throughout this paper unless otherwise stated.

- For a set \mathcal{A} , $|\mathcal{A}|$ denotes its cardinality.
- For positive integers a , b , and t with $a \leq b$ and $t \leq b$, we define $[a : b] \triangleq \{a, a+1, \dots, b\}$. Moreover, $\binom{[b]}{t} \triangleq \{\mathcal{A} \subseteq [b] \mid |\mathcal{A}| = t\}$ denotes the collection of all t -element subsets of $[b]$.
- For any $F \times K$ array \mathbf{P} , the entry in the f^{th} row and k^{th} column is denoted by $\mathbf{P}(f, k)$, where $f \in [F]$ and $k \in [K]$.

II. SYSTEM MODEL

In this section, we first introduce the MACC system with arbitrary user–cache access topology. Then, we present a graph-theoretic formulation of the MACC problem.

A. Multi-access coded caching

We consider the MACC system model [22], illustrated in Fig. 1, where a server has access to a library $\mathcal{W} = \{W_1, W_2, \dots, W_N\}$ of N equal-size files and is connected to K user nodes via an error-free broadcast link. The system contains Λ cache nodes, each of size M files. Unlike the shared-link setting, in which each user is associated with a dedicated cache, in the MACC

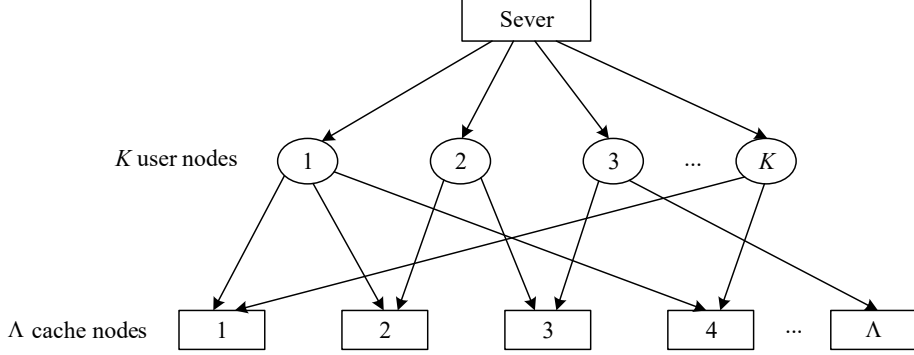


Fig. 1: MACC system model with arbitrary user-cache access topology.

model, each user $k \in [K]$ can access an arbitrary subset of cache nodes, denoted by $\mathcal{A}_k \subseteq [\Lambda]$. We refer to the collection $\mathcal{A} = \{\mathcal{A}_k \mid k \in [K]\}$ as the user–cache access topology.

A MACC scheme under an arbitrary user-cache access topology \mathcal{A} consists of two phases.

- **Placement phase:** Each file is divided into F packets of equal size. Without knowledge of future requests, each cache node $\lambda \in [\Lambda]$ stores a subset of packets from each file, subject to its storage constraint M . The content stored at cache node λ is denoted by \mathcal{Z}_λ . Each user $k \in [K]$ can retrieve all packets stored at the cache nodes in its accessible set \mathcal{A}_k , i.e., the accessible content by user k is $\mathcal{Z}_k = \bigcup_{\lambda \in \mathcal{A}_k} \mathcal{Z}_\lambda$.
- **Delivery phase:** Each user randomly requests one file. Let $\mathbf{d} = (d_1, d_2, \dots, d_K)$ denote the request vector. Based on \mathbf{d} , the cached contents \mathcal{Z}_λ , and the access topology \mathcal{A} , the server broadcasts $S_{\mathbf{d}}$ coded packets such that each user can recover its requested file using the received transmissions along with its accessible cache content \mathcal{Z}_k .

In this system, the worst-case number of transmitted files across all possible user requests (i.e., worst-case load) is defined as

$$R = \max_{\mathbf{d} \in [N]^K} \frac{S_{\mathbf{d}}}{F}, \quad (1)$$

which represents the normalized delivery load and should be minimized.

For the coded caching problem in the MACC system, a combinatorial framework called the MACC Placement Delivery Array (MACC-PDA) was proposed in [18] to systematically characterize MACC schemes. The MACC-PDA extends the concept of the Placement Delivery Array (PDA) originally introduced for the shared-link coded caching system with uncoded cache

placement and clique-covering-based delivery [4]. We briefly review the PDA framework below, as it serves as the foundation for the MACC-PDA construction.

Definition 1 (PDA, [4]). For any positive integers K, F, Z and S , an $F \times K$ array \mathbf{P} composed of a specific symbol “*” and S integers in $[S]$, is called a (K, F, Z, S) PDA if it satisfies the following conditions.

- C1. The symbol “*” appears Z times in each column; and
- C2. Each integer $s \in [S]$ appears at least once in the array;
- C3. For any two distinct entries $\mathbf{P}(f_1, k_1)$ and $\mathbf{P}(f_2, k_2)$, $\mathbf{P}(f_1, k_1) = \mathbf{P}(f_2, k_2) = s$ is an integer only if
 - a. $f_1 \neq f_2, k_1 \neq k_2$, i.e., they lie in distinct rows and columns; and
 - b. $\mathbf{P}(f_1, k_2) = \mathbf{P}(f_2, k_1) = *$, i.e., the corresponding 2×2 subarray formed by rows f_1, f_2 and columns k_1, k_2 must be of the following form

$$\begin{pmatrix} s & * \\ * & s \end{pmatrix} \quad \text{or} \quad \begin{pmatrix} * & s \\ s & * \end{pmatrix}. \quad (2)$$

Based on a (K, F, Z, S) placement delivery array (PDA), a F -division coded caching scheme for the (K, M, N) shared-link coded caching system can be constructed as follows.

- The K columns and F rows denote the users and packets of each file, respectively.
- The entry $\mathbf{P}(f, k) = *$ indicates that the f^{th} packet of all files is cached by user k . By Condition C1 of Definition 1, each user caches Z packets per file, which corresponds to a cache size of $M = \frac{ZN}{F}$ files.
- The entry $\mathbf{P}(f, k) = s$ denotes that the f^{th} packet of each file is not stored by user k . In the delivery phase, for each integer s , the server broadcasts a coded multicast message formed by the XOR of all requested packets indexed by s . By Condition C3 of Definition 1, each user involved in this multicast transmission can decode its requested packet, since it has cached all other packets in the corresponding XOR except the desired one.
- Let g_s denote the number of times the integer s appears in \mathbf{P} . Then g_s represents the coded caching gain at time slot s , meaning that the multicast transmission at time slot s is simultaneously useful for g_s users. By Condition C2 of Definition 1, the total number of multicast transmissions is S , and hence the normalized communication load is given by $R = \frac{S}{F}$.

In particular, if each integer in the PDA appears exactly g times, the PDA is said to be g -*regular*, and is denoted by g -(K, F, Z, S) PDA. The following lemma shows that the MN coded caching scheme corresponds to a specific PDA, referred to as the MN PDA.

Lemma 1. Given a (K, F, Z, S) PDA, there exists an F -division (K, M, N) shared-link coded caching scheme with the memory ratio $\frac{M}{N} = \frac{Z}{F}$ and load $R = \frac{S}{F}$.

Lemma 2. (MN PDA [2], [4]) For any positive integers K and t with $t < K$, there exists a $(t+1)$ -($K, \binom{K}{t}, \binom{K-1}{t-1}, \binom{K}{t+1}$) PDA.

Definition 2 (MACC-PDA, [18]). In an MACC system, the placement and delivery phases can be jointly represented using a structured array called an MACC-PDA. It composed of the node-placement array \mathbf{C} , user-retrieve array \mathbf{U} and user-delivery array \mathbf{Q} .

- **Node-placement array \mathbf{C} .** An $F \times \Lambda$ node-placement array \mathbf{C} consists of stars and nulls, where F and Λ represent the number of packets of each file and the number of cache nodes, respectively. For any $f \in [F]$ and $\lambda \in [\Lambda]$, the entry $\mathbf{C}(f, \lambda) = *$ if and only if the λ^{th} cache node stores the f^{th} packet of each file W_n .
- **User-retrieve array \mathbf{U} .** An $F \times K$ user-retrieve array \mathbf{U} consists of stars and nulls, where F and K represent the subpacketization of each file and the number of users, respectively. For any $f \in [F]$ and $\lambda \in [\Lambda]$, the entry $\mathbf{U}(f, k) = *$ if and only if the f^{th} packet of each file W_n is stored at least one cache node belonging to the user-cache access set \mathcal{A}_k .
- **User-delivery array \mathbf{Q} .** An $F \times K$ user-delivery array \mathbf{Q} consists of stars and integers in $[S]$, where the stars in \mathbf{Q} have the same meaning as the those in \mathbf{U} . Here, S denotes the total number of multicast messages transmitted by the server during the delivery phase, an integer entry $s \in [S]$ indicates that the corresponding packet is delivered via the s^{th} multicast transmission.

It has been shown in [18] that if the user-delivery array \mathbf{Q} in Definition 2 satisfies Condition C3 in Definition 1, then each user can successfully recover its requested file using its retrievable cache content and the received multicast packets.

Example 1. Consider an MACC system with $K = 5$ users and $\Lambda = 4$ cache nodes, as illustrated in Fig. 2. The transformation procedure from the node-placement array \mathbf{C} to the user-retrieve array \mathbf{U} and the user-delivery array \mathbf{Q} is shown in Fig. 3. The user-cache access topology is

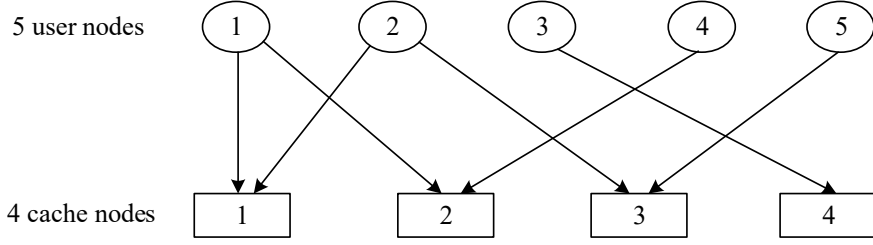


Fig. 2: User-cache access topology with 5 users and 4 cache nodes.

given by $\mathcal{A} = \{\mathcal{A}_k \mid k \in [5]\}$, where

$$\mathcal{A}_1 = \{1, 2\}, \mathcal{A}_2 = \{1, 3\}, \mathcal{A}_3 = \{4\}, \mathcal{A}_4 = \{2\}, \mathcal{A}_5 = \{3\}. \quad (3)$$

Each cache node stores the following subsets of packets according to the array \mathbf{P} in Fig 2,

$$\begin{aligned} \mathcal{Z}_1 &= \{W_{n,1}, W_{n,2}, W_{n,3} \mid n \in [6]\}, & \mathcal{Z}_2 &= \{W_{n,1}, W_{n,4}, W_{n,5} \mid n \in [6]\}, \\ \mathcal{Z}_3 &= \{W_{n,2}, W_{n,4}, W_{n,6} \mid n \in [6]\}, & \mathcal{Z}_4 &= \{W_{n,3}, W_{n,5}, W_{n,6} \mid n \in [6]\}. \end{aligned} \quad (4)$$

The corresponding node-placement array \mathbf{C} is obtained by extracting all star entries from the MN PDA \mathbf{P} . The user-retrieve array \mathbf{U} is then constructed from \mathbf{C} according to the user-cache access topology in (3). Specifically, the k^{th} column of \mathbf{U} is obtained by taking the union of the star entries in the columns of \mathbf{C} indexed by \mathcal{A}_k , i.e., $\mathbf{U}(f, k) = *$ if there exists some $\lambda \in \mathcal{A}_k$ such that $\mathbf{C}(f, \lambda) = *$. For example, since user 1 can access cache nodes $\mathcal{A}_1 = 1, 2$, the star entries in columns 1 and 2 of \mathbf{P} are given by

$$\mathbf{P}(1, 1) = \mathbf{P}(2, 1) = \mathbf{P}(3, 1) = *, \mathbf{P}(1, 2) = \mathbf{P}(4, 2) = \mathbf{P}(5, 2) = *. \quad (5)$$

As a result, the first column of \mathbf{U} satisfies

$$\mathbf{U}(1, 1) = \mathbf{U}(2, 1) = \mathbf{U}(3, 1) = \mathbf{U}(4, 1) = \mathbf{U}(5, 1) = *. \quad (6)$$

Finally, the user-delivery array \mathbf{Q} is constructed by filling the null entries of \mathbf{U} with integers such that Condition C3 in Definition 1 is satisfied. \square

However, existing schemes such as [18], [24], [29] are primarily tailored to specific user-cache

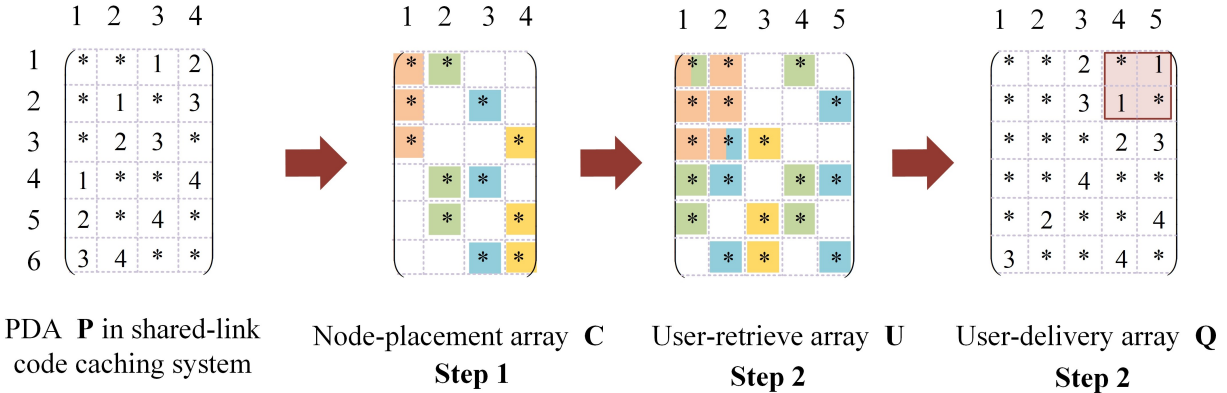


Fig. 3: Transformation from the MN PDA \mathbf{P} to an MACC scheme via arrays \mathbf{C} , \mathbf{U} , and \mathbf{Q} .

access topology. To the best of our knowledge, a general coded caching scheme that can accommodate MACC systems with arbitrary access topology is still lacking. This observation motivates us to investigate a more general and flexible design framework. In the following, we show that the user-delivery array \mathbf{Q} , constructed based on the user-retrieve array \mathbf{U} in Definition 2, can be reformulated as a graph coloring problem. This reformulation constitutes the foundation of our proposed approach. Specifically, for a given cache-node placement, the corresponding user-retrieve array \mathbf{U} can be directly obtained according to the user–cache access topology. Consequently, the design challenge reduces to determining the positions of the integer entries in the user-delivery array \mathbf{Q} based on the structure of \mathbf{U} .

B. Transformation from MACC–PDA to a graph coloring problem

We establish a graph-theoretic reformulation of the problem. Specifically, we show that designing the user-delivery array \mathbf{Q} in Definition 2, which characterizes the multi-access coded caching scheme, is equivalent to a graph coloring problem. This equivalence provides an efficient perspective and enables the utilization of well-established graph coloring methods. We first introduce the concept of graph coloring for undirected graphs, which is essential for the transformation from the MACC problem to a graph coloring problem.

Definition 3 (Undirected graph [39]). An undirected graph is an ordered pair $(\mathcal{V}, \mathcal{E})$, where \mathcal{V} is a finite and nonempty set of vertices, and $\mathcal{E} \subseteq \{\{u, v\} \mid u, v \in \mathcal{V}, u \neq v\}$ is a set of edges, where each edge connects two distinct vertices. We denote such a graph by $G = (\mathcal{V}, \mathcal{E})$. If $\{u, v\} \in \mathcal{E}$, then the vertices u and v are said to be adjacent.

With the concept of an undirected graph introduced above, we now present the definition of graph coloring.

Definition 4 (Graph coloring [39]). Let $G = (\mathcal{V}, \mathcal{E})$ be an undirected graph. We have the following properties.

- 1) A *proper coloring* of G is an assignment of colors to the vertices such that no two adjacent vertices are assigned the same color.
- 2) If a *proper coloring* of G uses k distinct colors, we call it a *k -coloring*, and say that G is *k -colorable*. The *chromatic number* of G , denoted by $\chi(G)$, is the minimum k for which G admits a k -coloring.

To design the user-delivery array \mathbf{Q} from the user-retrieve array \mathbf{U} , the key challenge lies in assigning integer entries to the null positions of \mathbf{U} such that Condition C3 in Definition 1 is satisfied. To this end, we construct a conflict graph $\mathcal{G} = (\mathcal{V}, \mathcal{E})$, which is an undirected graph as defined in Definition 3. In this graph, each vertex corresponds to one null entry in \mathbf{U} , and an edge is placed between two vertices if their corresponding entries violate Condition C3 in Definition 1. Consequently, non-adjacent vertices can be assigned the same color. In the resulting graph $\mathcal{G} = (\mathcal{V}, \mathcal{E})$, a *proper coloring* guarantees that adjacent vertices (i.e., conflicting entries) are assigned different colors, while non-adjacent vertices may share the same color. Therefore, finding a proper coloring of \mathcal{G} yields a valid assignment of integers to the null entries of \mathbf{U} that satisfies Condition C3. Since each color corresponds to one multicast transmission (i.e., one integer in the user-delivery array \mathbf{Q}), minimizing the number of colors is equivalent to minimizing the delivery load defined in (1). Hence, our objective is to determine the *chromatic number* of the graph \mathcal{G} .

In the following, we present an example to illustrate the detailed transformation from the user-retrieve array \mathbf{U} to the user-delivery array \mathbf{Q} from a graph coloring perspective.

Example 2. In this example, we consider a 3×3 user-retrieve array \mathbf{U} shown in Fig. 4(a), which consists of both star and null entries. The complete transformation procedure from \mathbf{U} to the user-delivery array \mathbf{Q} is illustrated in Fig. 4. The transformation consists of the following 4 steps.

- 1) **Vertex construction:** Each null entry $\mathbf{U}(f, k)$ in the user-retrieve array \mathbf{U} is mapped to a unique vertex $v_{f,k}$ in the undirected graph. Accordingly, the vertex set \mathcal{V} of graph \mathcal{G}

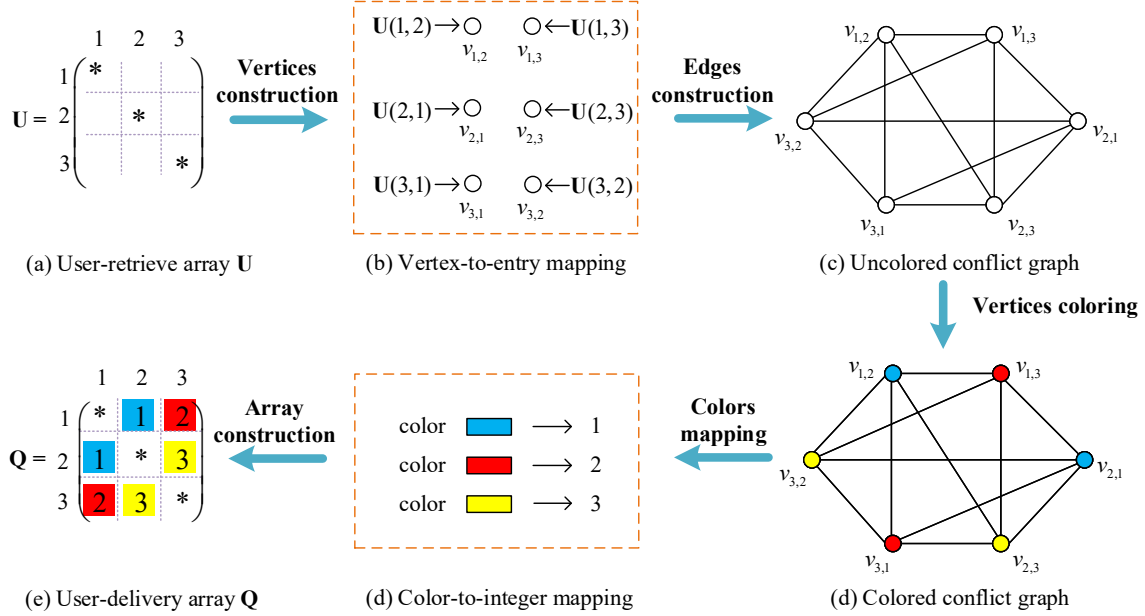


Fig. 4: Transformation from the user-retrieve array \mathbf{U} to the user-delivery array \mathbf{Q} in Example 2.

consists of all vertices corresponding to null entries in \mathbf{U} . In Fig. 4(a), there are six null entries, namely $\mathbf{U}(1,2)$, $\mathbf{U}(1,3)$, $\mathbf{U}(2,1)$, $\mathbf{U}(2,3)$, $\mathbf{U}(3,1)$, and $\mathbf{U}(3,2)$. Therefore, the vertex set is

$$\mathcal{V} = \{v_{1,2}, v_{1,3}, v_{2,1}, v_{2,3}, v_{3,1}, v_{3,2}\}, \quad (7)$$

as illustrated in Fig. 4(b).

2) **Edge construction:** Two vertices v_{f_1,k_1} and v_{f_2,k_2} are connected by an edge $\{v_{f_1,k_1}, v_{f_2,k_2}\} \in \mathcal{E}$ if and only if the corresponding entries $\mathbf{U}(f_1, k_1)$ and $\mathbf{U}(f_2, k_2)$ cannot simultaneously satisfy Condition C3 in Definition 1. Thus, the edge set \mathcal{E} consists of all pairs of vertices whose corresponding null entries are in conflict. For instance, for the null entry $\mathbf{U}(1,2)$, only its pairing with $\mathbf{U}(2,1)$ satisfies Condition C3, whereas all other pairings violate the condition. Hence, vertex $v_{1,2}$ is connected to vertices $v_{1,3}, v_{2,1}, v_{2,3}, v_{3,1}$, and $v_{3,2}$. Applying the

same rule to all vertices yields the set of edges listed in (8).

$$\begin{aligned}
v_{1,2} : & \{v_{1,2}, v_{1,3}\}, \{v_{1,2}, v_{2,3}\}, \{v_{1,2}, v_{3,1}\}, \{v_{1,2}, v_{3,2}\}; \\
v_{1,3} : & \{v_{1,3}, v_{1,2}\}, \{v_{1,3}, v_{2,1}\}, \{v_{1,3}, v_{2,3}\}, \{v_{1,3}, v_{3,2}\}; \\
v_{2,1} : & \{v_{2,1}, v_{1,3}\}, \{v_{2,1}, v_{2,3}\}, \{v_{2,1}, v_{3,1}\}, \{v_{2,1}, v_{3,2}\}; \\
v_{2,3} : & \{v_{2,3}, v_{1,2}\}, \{v_{2,3}, v_{1,3}\}, \{v_{2,3}, v_{2,1}\}, \{v_{2,3}, v_{3,1}\}; \\
v_{3,1} : & \{v_{3,1}, v_{1,2}\}, \{v_{3,1}, v_{2,1}\}, \{v_{3,1}, v_{2,3}\}, \{v_{1,3}, v_{3,2}\}; \\
v_{3,2} : & \{v_{3,2}, v_{1,2}\}, \{v_{3,2}, v_{1,3}\}, \{v_{3,2}, v_{2,1}\}, \{v_{3,2}, v_{3,1}\}.
\end{aligned} \tag{8}$$

Since the graph is undirected, each edge is unordered, and the complete edge set \mathcal{E} is given by

$$\begin{aligned}
\mathcal{E} = & \{\{v_{1,2}, v_{1,3}\}, \{v_{1,2}, v_{2,3}\}, \{v_{1,2}, v_{3,1}\}, \{v_{1,2}, v_{3,2}\}, \{v_{1,3}, v_{2,1}\}, \{v_{1,3}, v_{2,3}\}, \\
& \{v_{1,3}, v_{3,2}\}, \{v_{2,1}, v_{2,3}\}, \{v_{2,1}, v_{3,1}\}, \{v_{2,1}, v_{3,2}\}, \{v_{2,3}, v_{3,1}\}, \{v_{3,2}, v_{3,1}\}\}.
\end{aligned} \tag{9}$$

3) **Graph coloring:** Following Definition 4, colors are assigned to the vertices of \mathcal{G} such that adjacent vertices receive different colors, while non-adjacent vertices may share the same color. By construction, non-adjacent vertices correspond to entries that already satisfy Condition C3. Vertices $v_{1,2}$ and $v_{2,1}$ are non-adjacent and are therefore assigned the same color. Proceeding similarly for all vertices and mapping colors to integers yields

$$C(v_{1,2}) = C(v_{2,1}) = 1, \quad C(v_{1,3}) = C(v_{3,1}) = 2, \quad C(v_{2,3}) = C(v_{3,2}) = 3. \tag{10}$$

4) **Array construction:** Finally, according to the vertex index (f, k) and its assigned color s , the color s is placed in the corresponding entry $\mathbf{U}(f, k)$, producing the user-delivery array \mathbf{Q} . Specifically, in this example, $\mathbf{Q}(1, 2) = \mathbf{Q}(2, 1) = 1$, $\mathbf{Q}(1, 3) = \mathbf{Q}(3, 1) = 2$, and $\mathbf{Q}(2, 3) = \mathbf{Q}(3, 2) = 3$. As shown in [4], the resulting array \mathbf{Q} achieves the minimum delivery load in (1). Equivalently, the graph \mathcal{G} admits a proper coloring with chromatic number $\chi(\mathcal{G}) = 3$.

□

Inspired from the above example, we obtain the following result.

Remark 1. The chromatic number $\chi(\mathcal{G})$ of the conflict graph $\mathcal{G} = (\mathcal{V}, \mathcal{E})$ is equal to the minimum delivery load defined in (1) achieved by the corresponding user-delivery array \mathbf{Q} .

Based on the above transformation, the construction of the user-delivery array \mathbf{Q} can be equivalently interpreted as a graph coloring problem on the conflict graph $\mathcal{G} = (\mathcal{V}, \mathcal{E})$. Consequently, the MACC delivery design problem reduces to finding a *proper coloring* of \mathcal{G} using as few colors as possible, i.e., a *k-coloring* with a minimum k . However, determining the exact *chromatic number* of an arbitrary graph \mathcal{G} is a well-known NP-hard combinatorial optimization problem in graph theory [40]. As a result, computing the optimal user-delivery array \mathbf{Q} via exact graph coloring becomes computationally prohibitive for large-scale MACC systems.

C. Main objective of the paper

The objective of this paper is to develop a general and low-complexity delivery scheme with the MN cache placement at the cache nodes,¹ for arbitrary user–cache access topology.

In addition, with the MN cache placement, we also aim to establish a general and low-complexity converse bound on the transmission load for arbitrary user–cache access topology.

III. PRELIMINARY

In this section, we review the graph coloring approaches [43]–[47], the Potts model [48], and GNNs architectures [49]. In addition, we extend the IC converse bound on the delivery load developed in [3] to the MACC problem considered in this paper.

A. Classical graph coloring

A wide range of graph coloring algorithms have been studied in the literature, including local search-based methods such as tabu search [50] and evolutionary algorithms. While these methods can achieve good performance in certain settings, they are often sensitive to algorithmic parameters. Consequently, they may incur substantial computational overhead and fail to consistently produce high-quality solutions, especially for large-scale or structurally complex graphs. Greedy heuristics are generally more efficient. Among them, the DSatur algorithm [43] is a widely used greedy coloring method that dynamically selects vertices according to their saturation degree (SD), defined as the number of distinct colors assigned to neighboring vertices. By prioritizing

¹In this paper, we adopt the MN uncoded placement strategy at the cache nodes, which is commonly used in the multi-access coded caching (MACC) literature [18], [21], [23], [24], [41], [42]. Notably, for cyclic wrap-around access topology (which is the most commonly considered user–cache access topology in MACC coded caching), it was established in [18] that schemes derived via a transformation of the MN placement achieve the maximum local caching gain. Moreover, when $K \gg tL$, where t denotes the number of users caching each packet of a file and L denotes the number of neighboring cache nodes connected to each user, the resulting scheme is approximately optimal.

the most constrained vertices, DSatur effectively captures local coloring constraints and typically produces colorings close to the *chromatic number* $\chi(G)$ for the conflict graph $\mathcal{G} = (\mathcal{V}, \mathcal{E})$ in the MACC delivery problem. Thus it serves as a strong benchmark for learning-based approaches, as validated in Sections V and VI. The procedure is summarized in Algorithm 1.

Algorithm 1 DSatur algorithm for graph coloring [43]

```

1: Input: An undirected graph  $G = (\mathcal{V}, \mathcal{E})$ 
2: Output: A proper coloring  $C(v)$  for all  $v \in \mathcal{V}$ 
3: Initialization: Set  $C(v) = 0$ ,  $SD(v) = 0$  for all  $v \in \mathcal{V}$ , the uncolored vertex set  $\mathcal{U} \leftarrow \mathcal{V}$ ;
   record the degree  $D(v)$  and neighbor set  $\mathcal{N}(v)$ 
4: while  $\mathcal{U} \neq \emptyset$  do
5:    $SD_{\max} \leftarrow \max_{v \in \mathcal{U}} SD(v)$ 
6:    $\mathcal{U}' \leftarrow \{v \in \mathcal{U} \mid SD(v) = SD_{\max}\}$ 
7:   if  $|\mathcal{U}'| > 1$  then
8:     Select  $u \leftarrow \arg \max_{v \in \mathcal{U}'} D(v)$ 
9:   else
10:    Select  $u \in \mathcal{U}'$ 
11:   end if
12:   Assign  $C(u) \leftarrow \min\{i \in \mathbb{N}^+ \mid \forall w \in \mathcal{N}(u), C(w) \neq i\}$ 
13:    $\mathcal{U} \leftarrow \mathcal{U} \setminus \{u\}$ 
14:   for  $v \in \mathcal{N}(u)$  do
15:     Update  $SD(v)$ 
16:   end for
17: end while

```

Computational complexity of DSatur: Although DSatur provides a strong heuristic for graph coloring, its computational complexity becomes prohibitive in MACC systems with a large number of user nodes. In general, DSatur incurs a time complexity on the order of $\mathcal{O}(|\mathcal{V}|^2 + |\mathcal{E}|)$, due to repeated searches over uncolored vertices and frequent updates of saturation degrees for adjacent vertices. In the MACC-to-graph-coloring formulation in Section II-B, the vertices of the conflict graph correspond to the null entries of the user–retrieve array \mathbf{U} . Under the MN uncoded placement, each file is partitioned into $F = \binom{K}{t}$ packets, where $t \in \{0, 1, \dots, K\}$. In the worst case of arbitrary access, the number of vertices satisfies $|\mathcal{V}| \leq KF = K\binom{K}{t} = \mathcal{O}(K^{t+1})$ which

grows exponentially with the number of users. Consequently, the time complexity of DSatur can be upper bounded as $\mathcal{O}(|\mathcal{V}|^2 + |\mathcal{E}|) = \mathcal{O}((K \binom{K}{t})^2 + |\mathcal{E}|)$. Moreover, the strong decoding constraints specified in Definition 1 induce a large number of conflicts among vertices, rendering the resulting conflict graphs typically dense. Consequently, the runtime of DSatur grows rapidly with the number of user nodes, which motivates the development of low-complexity solutions for MACC problems.

B. GNN-based graph coloring

GNNs have recently emerged as a promising learning-based approach for graph coloring, particularly for large-scale or structurally complex graphs where classical heuristic algorithms may suffer from high computational complexity or degraded performance. By leveraging message-passing mechanisms, GNNs can learn expressive vertex embeddings that capture both local neighborhood information and global graph structure.

Existing GNN-based graph coloring methods can be broadly categorized according to their optimization objectives and generalization settings. Some works focus on *single-graph optimization*, where the learning model is trained and evaluated on the same target graph. For example, a population-based framework was proposed in [44] that iteratively refines candidate colorings for a given graph. While such approaches can achieve strong performance on a fixed graph instance, the learned models are tightly coupled to that specific graph and are not designed to generalize across graphs with varying sizes or topology. Other learning-based approaches consider relaxed or indirect formulations of the graph coloring problem. For instance, Graph Discrimination Networks (GDNs) in [51], Potts-based approaches in [46] and Minimal Cost Graph Neural Network (MCGNN) [52] learn representations related to coloring constraints but do not explicitly guarantee conflict-free color assignments. The work in [53], on the other hand, focuses on predicting the chromatic number rather than constructing a *proper coloring*. There also exist hybrid methods that combine GNN-based predictions with post-processing heuristics, such as tabu search, to resolve coloring conflicts [47]. While these approaches can improve solution quality and generalization performance, their reliance on iterative local search introduces significant computational overhead, which may become prohibitive for large-scale or dynamically generated graphs.

Limitations of existing GNN-based coloring approaches: Overall, existing GNN-based graph coloring methods exhibit a fundamental tradeoff between solution quality, generalization capabil-

ity, and computational efficiency. In particular, limited cross-graph generalization and the reliance on iterative post-processing are recurring limitations in current learning-based approaches. These observations motivate the development of alternative GNN-based formulations that better balance accuracy, generality, and computational cost.

C. Converse bound based on index coding

The converse bound under uncoded cache placement developed in [3] establishes a fundamental connection between coded caching and index coding (IC) [54]. Specifically, when the cache placement phase is uncoded and both the cache contents and user demands are fixed, the delivery phase of a caching system can be equivalently viewed as an index coding problem. In the considered MACC setting, for given MN cache-node placement and user-cache access topology \mathcal{A} , the cache contents available to each user can be uniquely determined. Therefore, the IC converse framework in [3] can be directly applied to derive a lower bound on the delivery load of the MACC problem.

The work in [3] shows that, for any given demand vector and user permutation, an acyclic set of subfiles can be constructed to yield a linear inequality on the delivery load, expressed as the sum of the lengths of the subfiles in the selected acyclic set. The overall converse bound is then obtained by aggregating such inequalities over all possible demand vectors and user permutations.

Lemma 3 (Converse bound [3]). Consider a MACC system with K users, Λ cache nodes, and an arbitrary user-cache access topology. Let $\mathcal{A}_k \subseteq [\Lambda]$ denote the set of cache nodes accessible to user $k \in [K]$, and let $\mathbf{d} = (d_1, d_2, \dots, d_K)$ denote a demand vector. For any user permutation $\mathbf{u} = (u_1, \dots, u_K)$, the transmission load satisfies

$$R_{\mathbf{u}} \geq \sum_{i \in [K]} \sum_{\mathcal{J}_{u_i} \subseteq [\Lambda] \setminus \bigcup_{j=1}^i \mathcal{A}_{u_j}} \frac{|W_{d_{u_i}, \mathcal{J}_{u_i}}|}{F}, \quad (11)$$

where $W_{d_{u_i}, \mathcal{J}_{u_i}}$ denotes a packet of the file requested by user u_i that is cached exclusively at cache nodes indexed by \mathcal{J}_{u_i} . The worst-case delivery load under uncoded cache placement is bounded by

$$R \geq \max_{\mathbf{u} \in \mathfrak{U}} R_{\mathbf{u}} \quad (12)$$

where \mathfrak{U} denotes the set of all user permutations. \square

The inequality in (11) corresponds to a single acyclic-set inequality associated with a specific demand vector \mathbf{d} and user permutation \mathbf{u} , and follows directly from the IC converse by constructing an acyclic set according to the permutation order \mathbf{u} . The inner summation is taken over all packet index sets \mathcal{J}_{u_i} that are not accessible through the cache nodes available to the first i users in the permutation order \mathbf{u} . Under uncoded cache placement, each file is partitioned according to the same collection of packet index sets, independent of the file index. As a result, for any fixed packet index set \mathcal{J} , the corresponding packets $\{W_{n,\mathcal{J}} \mid n \in [N]\}$ have identical cache placement and induce the same side-information structure in the associated index coding problem. Consequently, different demand vectors lead to acyclic-set inequalities of the same form in (11). This demand symmetry implies that the inequalities in (11) depend only on the user permutation \mathbf{u} and the cache-access topology \mathcal{A} , but not on the specific files requested. Therefore, we only consider the demand vectors with distinct requested files when evaluating the converse bound. By taking the maximum of (11) over all user permutations \mathbf{u} and over all demand vectors with distinct requested files, we obtain a converse bound on the worst-case delivery load of the MACC system (see (12)).

Evaluating the converse bound in Lemma 3 requires enumerating all user permutations (i.e., $K!$ permutations), and all packets index sets \mathcal{J}_{u_i} for each $i \in [K]$. Consequently, the number of inequalities grows factorially with the number of users K and combinatorially with Λ and t , resulting in a computational complexity on the order of

$$\mathcal{O}\left(|\mathfrak{U}| \cdot \sum_{i=1}^K \binom{\Lambda}{t}\right) = \mathcal{O}\left(|\text{Perm}(K, K)| \cdot \sum_{i=1}^K \binom{\Lambda}{t}\right). \quad (13)$$

For example, when $N = K = 3$, there are $|\mathfrak{U}| = 3! = 6$ distinct inequalities, and this number increases rapidly as K grows. This prohibitive complexity motivates the development of low-complexity approaches to approximate the converse bound, which we address in Section V via a greedy algorithm.

IV. AI-AIDED FRAMEWORK FOR MACC SYSTEMS WITH ARBITRARY TOPOLOGIES

Designing the delivery phase of an MACC system with arbitrary cache–user topology is a challenging problem. As discussed in Section II-A, even for regular topology, traditional approaches rely on manually constructing the MACC-PDA user-delivery array \mathbf{Q} by carefully transforming the user-retrieval array \mathbf{U} to satisfy Condition C3 in Definition 1. Such constructions

are inherently discrete and non-convex such that the delivery design is a difficult problem. Moreover, for the classical graph coloring approaches, the delivery phase must be redesigned for each cache-user topology. To address this challenge, Section III-A shows that the delivery design problem can be equivalently formulated as a graph coloring problem on the induced conflict graph. Classical heuristic algorithms, such as the DSatur algorithm in Algorithm 1, provide a solution framework. However, the size of the conflict graph grows exponentially with the number of user nodes, (with the number of vertices scaling as $|\mathcal{V}| \leq \mathcal{O}(K^{t+1})$, where $t \in \{0, 1, \dots, K\}$). As a result, the computational complexity of applying such heuristic coloring algorithms becomes prohibitively high in large-scale MACC systems, severely limiting their practical applicability.

These challenges motivate the adoption of data-driven, learning-based methods, such as GNNs, which offer an alternative for automatically learning low-complexity delivery strategies and generalizing across arbitrary cache-user topology. While existing GNN-based graph coloring approaches, however, often optimize color assignments on fixed graphs or rely on computationally expensive inference procedures [45], [46], [52], which limits the applicability to large-scale and dynamically generated conflict graphs in MACC systems. Furthermore, many learning-based graph coloring methods are typically trained and evaluated on graphs drawn from a fixed or moderately varying distribution, where the underlying graph structures are assumed to be statistically regular. In contrast, the conflict graphs arising in MACC systems are induced by MACC-PDA constructions and arbitrary cache–user access topology, resulting in a family of graphs whose structural properties are difficult to characterize a priori. This variability results in additional challenges for generalization and calls for a learning-based framework that can robustly handle such diverse graph structures.

Overall, the above fact motivates us to design a universal AI-based coloring framework for the MACC problem with arbitrary cache–user access topology, which has a significantly lower complexity than the existing schemes and achieves a performance approaching the converse bound.

A. *Overview of the proposed framework*

We propose an AI-aided framework to optimize the delivery phase in MACC systems with general cache-user access patterns. This framework contains three main steps, as illustrated in Fig. 5. Step 1, detailed in Section II-B, transforms the MACC-PDA problem into an equivalent conflict graph formulation. Step 2 employs a GNN to predict color assignments for the vertices

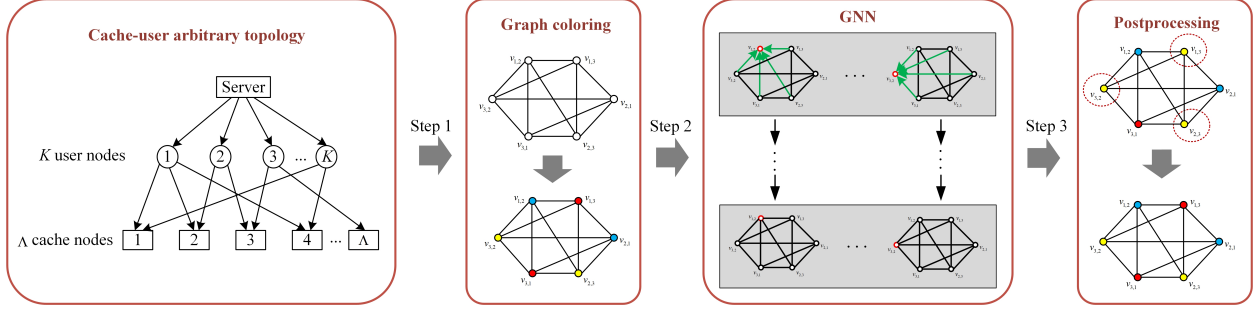


Fig. 5: AI-aided framework for the delivery phase in MACC systems with arbitrary user–cache access topology.

of the conflict graph. Step 3 applies a lightweight post-processing procedure to ensure that the predicted coloring corresponds to a feasible delivery scheme. By combining learning-based predictions with structured post-processing, the framework achieves low-complexity delivery design with strong generalization across arbitrary cache–user topology.

Note that the details of Step 1 have been described in Section II-B. In the following, we will introduce the details of Steps 2 and 3.

B. Step 2: GNN-Based color prediction

In this step, the conflict graph obtained from Step 1 serves as the input to GNNs that predicts color assignments for each vertex. The step consists of the following components. Although *proper coloring* must be globally conflict-free, the vertices coloring are determined by its neighbors due to decoding constraints. For the learning-based coloring approach, it is unnecessary to capture highly expressive or graph-level structural representations. Instead, an effective predictor should focus on the local conflicts and generating color assignments that are consistent with the decoding constraints. Motivated by this task-specific requirement, the proposed GNN is designed as a lightweight local-decision model. The neighbor-enhanced message-passing mechanism emphasizes relevant neighbors, while the embedding-based color projection relaxes discrete coloring into a continuous space that facilitates learning and allows efficient post-processing. This design enables the GNN to generate color predictions that are already close to feasible solutions, achieving near-optimal performance with substantially reduced computational complexity.

The step consists of the following components.

a) *Input Representation and Preprocessing*: To enable the GNN to design the delivery phase in the MACC system, the coded caching scheme and network topology are first encoded as a graph $\mathcal{G} = (\mathcal{V}, \mathcal{E})$. Each vertex $v \in \mathcal{V}$ represents a transmitted packet, while each edge $(u, v) \in \mathcal{E}$ denotes a conflict between two transmissions, i.e., the corresponding users do not cache each other's requested packets, resulting in non-decodable interference as specified by Condition C3 in Definition 1. The goal is to assign colors to the vertices such that adjacent vertices receive different colors while minimizing the total number of colors used. Each color assignment corresponds to a group of packets that can be transmitted simultaneously, thereby enabling an efficient delivery phase.

In our graph coloring formulation, the color of a vertex depends on the colors of its neighbors, making structural connectivity critical for learning effective coloring strategies. For each vertex v , we extract a feature vector $\mathbf{x}_v \in \mathbb{R}^1$ capturing its local structural properties. Specifically, we define $\mathbf{x}_v = [D(v)]$, where $D(v)$ denotes the degree of vertex v , i.e., the number of neighboring vertices (Although $D(v)$ is a scalar, it is represented as a one-dimensional feature vector to conform to the standard input format of GNNs.). All vertex features are stacked into a feature matrix

$$\mathbf{X} = [\mathbf{x}_1; \mathbf{x}_2; \dots; \mathbf{x}_{|\mathcal{V}|}] \in \mathbb{R}^{|\mathcal{V}| \times 1}, \quad (14)$$

and standardized using the global mean and variance computed from the training set to ensure consistent scaling across different graphs. The adjacency structure of the graph is encoded as an edge index $\mathbf{e} \in \mathbb{Z}^{2 \times |\mathcal{E}|}$, which lists all pairs $(u, v) \in \mathcal{E}$ in the PyTorch Geometric sparse format. The vertex label vector \mathbf{y} contains the color indices obtained from the DSatur algorithm. Consequently, each graph can be represented as a PyTorch Geometric data object

$$\text{Data}(x = \mathbf{X}, \text{edge_index} = \mathbf{e}, y = \mathbf{y}). \quad (15)$$

This preprocessing pipeline provides the GNN with a standardized and structurally informative representation of each graph. By ensuring consistent feature scaling and universal data formatting, it stabilizes optimization and promotes reliable learning across diverse network topology. With these structured representations, the GNN can effectively learn end-to-end coloring strategies for the MACC delivery phase, leveraging both local vertex patterns and global graph properties to achieve efficient transmission scheduling.

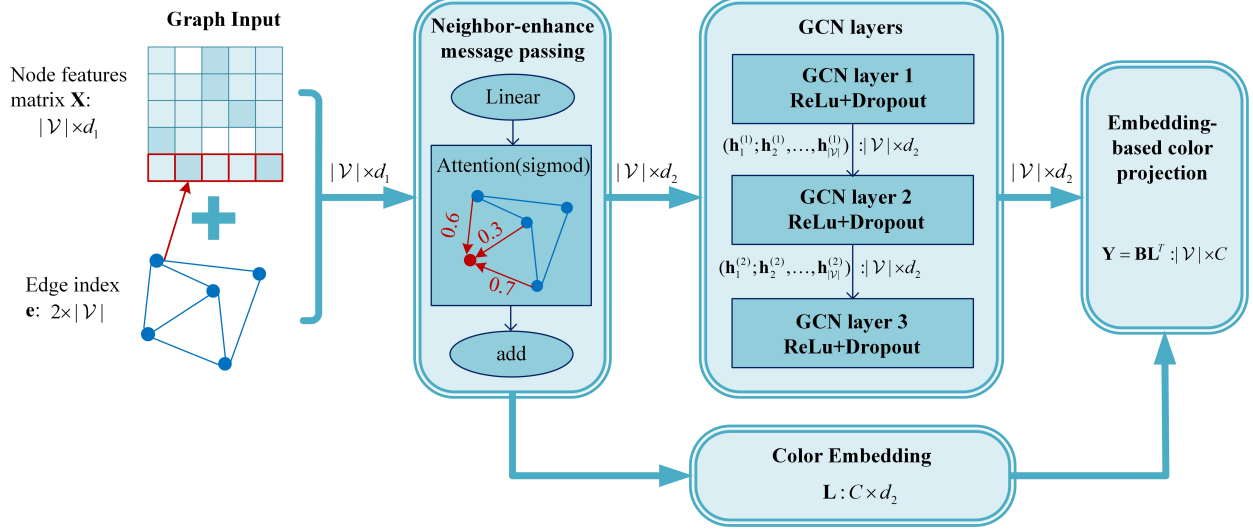


Fig. 6: Overall architecture of the proposed GNN model for graph coloring in MACC systems. The model consists of (i) a neighbor-enhanced message-passing module, (ii) three stacked GCN layers, and (iii) an embedding-based color projection head.

b) Model Architecture: Our GNN model builds upon the standard message-passing framework and is specifically designed to learn *proper colorings* for graphs arising from MACC systems with arbitrary topology. Given a graph $\mathcal{G} = (\mathcal{V}, \mathcal{E})$, the network outputs, for each vertex, a soft assignment over a predefined set of color classes, which can later be projected to a discrete coloring. The architecture is thus designed to (i) capture neighborhood structures that directly influence coloring decisions and (ii) enable differentiable color assignment through an embedding-based output layer. Fig. 6 illustrates the overall architecture.

Neighbor-enhanced message passing: Although the underlying graph is undirected, message passing treats each neighbor-target pair (u, v) as a directed dependency for aggregation. Unlike standard GCNs that aggregate neighbors uniformly, our *NeighborMessagePassing* module adaptively reweights incoming messages using learnable attention coefficients. This allows the model to emphasize neighbors whose colors impose stronger constraints on the valid coloring of vertex v . Formally, let $\mathbf{x}_v \in \mathbb{R}^F$ denote the input feature of vertex v (in our case, $F = 1$, corresponding to vertex degree). For each edge $u \rightarrow v$, the message is first transformed via a learnable linear map

$$\mathbf{m}_{u \rightarrow v} = \mathbf{W}_m \mathbf{x}_u \in \mathbb{R}^d, \quad (16)$$

where $\mathbf{W}_m \in \mathbb{R}^{d \times F}$ is trainable. An attention score is then computed as

$$\mathbf{s}_{u \rightarrow v} = \sigma(\mathbf{a}^T \mathbf{m}_{u \rightarrow v}) \in (0, 1), \quad (17)$$

where $\mathbf{a} \in \mathbb{R}^d$ is a learnable attention vector and $\sigma(\cdot)$ is the sigmoid function ². The weighted message is $\tilde{\mathbf{m}}_{u \rightarrow v} = \mathbf{s}_{u \rightarrow v} \mathbf{m}_{u \rightarrow v}$. Messages from all neighbors are aggregated by summation, i.e.,

$$\mathbf{m}_v = \sum_{u \in \mathcal{N}(v)} \tilde{\mathbf{m}}_{u \rightarrow v} = \sum_{u \in \mathcal{N}(v)} \mathbf{s}_{u \rightarrow v} \mathbf{W}_m \mathbf{x}_u. \quad (18)$$

This attention-weighted aggregation allows the network to focus on structurally influential neighbors, producing discriminative vertex representations for coloring.

GCN layers: The proposed model employs multiple stacked graph convolutional network (GCN) layers to perform message passing on the conflict graph induced by the MACC-PDA. In a GCN, each vertex iteratively aggregates information from its neighboring vertices, enabling the learning of structure-aware embeddings that are well suited for graph coloring tasks. Formally, let $\mathbf{h}_v^{(l)}$ denote the embedding of vertex v at the l -th layer. A GCN layer updates the embedding as

$$\mathbf{h}_v^{(l)} = \sigma \left(\sum_{u \in \mathcal{N}(v) \cup \{v\}} \frac{1}{\sqrt{d_v d_u}} \mathbf{W}^{(l)} \mathbf{h}_u^{(l-1)} \right), \quad (19)$$

where $\mathcal{N}(v)$ denotes the set of neighbors of v , d_v is the degree of vertex v , $\mathbf{W}^{(l)}$ is a trainable weight matrix, and $\sigma(\cdot)$ represents a nonlinear activation function. This formulation allows each vertex to aggregate normalized information from its local neighborhood, such that the resulting embeddings reflect the underlying graph structure relevant for coloring decisions. By stacking multiple GCN layers, the receptive field of each vertex is progressively expanded, enabling the model to incorporate both local interactions and higher-order structural dependencies in large and dense MACC conflict graphs. In our implementation, three GCN layers with ReLU activations and dropout are employed, producing expressive vertex embeddings that serve as the basis for subsequent color assignment.

Embedding-based color projection: To map vertex embeddings to color predictions, the model uses an embedding-based output layer instead of a standard linear classifier. Each color

²We use the sigmoid function instead of softmax to compute neighbor message weights independently. This prevents nodes with many neighbors from diluting the contributions of individual edges, preserves each edge's influence, and ensures stable gradients during training.

class is associated with a learnable embedding vector, and the output logits are computed as inner products between vertex embeddings and color embeddings. By embedding both vertices and colors into a shared space, the model can capture similarity relationships among color assignments and produce smooth, differentiable output distributions.

Let $\mathbf{b}_v = \mathbf{h}_v^{(3)} \in \mathbb{R}^d$ denote the final embedding of vertex v from the third GCN layer, and $\mathbf{L} \in \mathbb{R}^{C \times d}$ the learnable color embeddings matrix for C colors. The output logits for vertex v are $\mathbf{y}_v = \mathbf{b}_v \mathbf{L}^T \in \mathbb{R}^C$. For the full graph, stacking all vertex embeddings yields

$$\mathbf{Y} = (\mathbf{y}_1; \mathbf{y}_2; \dots; \mathbf{y}_{|\mathcal{V}|}) = \mathbf{BL}^T \in \mathbb{R}^{|\mathcal{V}| \times C}. \quad (20)$$

Overall, the architecture, comprising the neighbor-enhanced message-passing module, three GCN layers, and the embedding-based color projection, enables the model to learn expressive vertex embeddings and produce high-quality graph colorings, making it well-suited for designing efficient delivery phases in MACC systems.

c) *GNN Training*: The proposed GNN model is trained in an unsupervised manner to learn *proper colorings* of the conflict graphs arising from the MACC delivery phase with arbitrary cache–user access topology. Standard supervised training using color assignments from the DSatur algorithm is problematic because the numerical indices of color classes are arbitrary, any permutation of color labels constitutes a valid coloring as long as adjacent vertices receive distinct colors. Consequently, a supervised loss such as cross-entropy would incorrectly penalize valid solutions. To address this, we adopt a Potts-inspired unsupervised training strategy. The Potts model [46] provides a natural physical formulation for graph coloring, i.e., adjacent vertices sharing the same color contribute positive energy, while distinct colors contribute none. For a graph $\mathcal{G} = (\mathcal{V}, \mathcal{E})$, the discrete Potts Hamiltonian can be expressed as

$$H_{\text{Potts}} = J \sum_{\{u,v\} \in \mathcal{E}} \delta(s_u = s_v), \quad (21)$$

where s_v denotes the discrete color of vertex v and $J > 0$ is the interaction strength.

To enable gradient-based optimization with GNN outputs, we relax the discrete variables to continuous soft assignments. Each vertex v is associated with a probability vector $\mathbf{p}_v(\theta) \in [0, 1]^C$, produced via a softmax transformation of the GNN outputs, where $[\mathbf{p}_v]_c$ represents the probability

of assigning color c . The corresponding differentiable Potts-inspired loss becomes

$$\mathcal{L}_{\text{Potts}}(\theta) = -J \sum_{\{u,v\} \in \mathcal{E}} \mathbf{p}_u^T \mathbf{p}_v. \quad (22)$$

Minimizing this loss reduces the probability of adjacent vertices sharing the same color, enforcing proper coloring while remaining invariant to permutations of color indices.

While the Potts loss ensures local coloring consistency, it does not regulate the total number of colors used, which directly affects the number of transmissions in the MACC delivery phase. To encourage efficiency, we introduce a color-count regularization term that penalizes deviations between the estimated number of active colors in the soft assignments and the color number obtained from the DSatur algorithm. The overall training objective is thus

$$\mathcal{L}_{\text{total}}(\theta) = \mathcal{L}_{\text{Potts}}(\theta) + \beta \mathcal{L}_{\text{color-count}}(\theta), \quad (23)$$

where β balances the edge-level and global objectives. This combined loss enables the GNN to learn feasible, efficient colorings that respect the structure of the MACC delivery problem.

d) Training procedure: The GNN parameters θ are optimized end-to-end using batch stochastic gradient descent. In each training iteration, a batch of graphs $\{G_B\}$ is merged into a single disconnected graph via PyTorch Geometric's batching operator, which preserves the subgraph indices through the batch vector. Given the predicted color logits \mathbf{Y} , the training loss is computed according to the formulation in (23). Gradients are backpropagated, and parameters are updated using the AdamW optimizer with an initial learning rate η and weight decay λ . A cosine annealing scheduler is applied to gradually decrease the learning rate over training epochs. To stabilize optimization, a temperature parameter τ is applied to the softmax operator that converts logits into relaxed color probabilities. A smaller temperature prevents the model from making overly confident early predictions, resulting in smoother gradients and more stable training. The global color-count regularization term is weighted by β . The number of available colors C for each graph is dynamically determined by the distinct color count from the DSatur algorithm in the batch, allowing the model to adapt to graphs with varying chromatic structures.

The model outputs a probability distribution over the available colors for each vertex. These soft predictions are converted into discrete color labels by assigning each vertex $v \in \mathcal{V}$ the color

with the highest predicted probability

$$C(v) = \arg \max_{c \in \{1, \dots, C\}} p_{v,c}, \quad (24)$$

where $p_{v,c}$ denotes the predicted probability of assigning color c to vertex v . Since the training loss only penalizes color conflicts softly, the argmax assignment may still produce conflicting edges

$$\mathcal{E}_{\text{conf}} = \{\{u, v\} \in \mathcal{E} \mid C(u) = C(v)\}. \quad (25)$$

Therefore, a postprocessing step is applied to resolve remaining conflicts and produce a *proper coloring* for the graph.

C. Step 3: Postprocessing

After training, the GNN produces an initial vertex coloring that may still contain conflicts, i.e., some adjacent vertices may be assigned the same color. To obtain a *proper coloring*, we apply a postprocessing procedure, summarized in Algorithm 2. It uses first-fit color selection strategy in Algorithm 3 to efficiently assign colors while controlling the total number of colors used.

a) *Conflict Repair*: The algorithm first identifies all vertices whose current color assignments violate the coloring constraints. For each conflict vertex, the SD is computed. Conflict vertices are then processed in decreasing order of saturation degree. Each vertex is recolored using the Color Select procedure (Algorithm 3), which assigns the smallest available color not used by neighboring vertices, or introduces a new color if necessary.

b) *Color Selection*: The Color Select procedure (Algorithm 3) implements a first-fit strategy, selecting the minimum color not used by neighbors or adding a new color if all existing colors conflict. This strategy ensures that conflicts are efficiently resolved while minimizing the total number of colors.

Example 3. We illustrate the conflict repair procedure with a simple example. As shown in Fig. 7, the initial coloring is given by

$$C = \{C(v_{1,2}) = 1, C(v_{1,3}) = 2, C(v_{2,1}) = 1, C(v_{2,3}) = 3, C(v_{3,1}) = 3, C(v_{3,2}) = 2\}. \quad (26)$$

The set of used colors is $\mathcal{C}_{\text{used}} = \{1, 2, 3\}$, and the set of conflicted vertices is $\mathcal{V}_{\text{conf}} = \{v_{1,3}, v_{2,1}, v_{3,2}\}$. Since all vertices in $\mathcal{V}_{\text{conf}}$ have the same SD , the first-fit strategy is applied to break ties, i.e.,

Algorithm 2 Conflict Repair Procedure

- 1: **Input:** Graph $\mathcal{G} = (\mathcal{V}, \mathcal{E})$, initial coloring C
- 2: **Output:** A proper coloring C
- 3: Collect used colors $\mathcal{C}_{\text{used}} \leftarrow \{C(v) \mid v \in \mathcal{V}\}$
- 4: Identify conflict vertices $\mathcal{V}_{\text{conf}} \leftarrow \{v \mid \exists(u, v) \in \mathcal{E}, C(u) = C(v)\}$
- 5: **Global Conflict Repair**
- 6: **if** $\mathcal{V}_{\text{conf}} \neq \emptyset$ **then**
- 7: Compute saturation degree $SD(v) = |\{C(u) \mid u \in \mathcal{N}(v)\}|$
- 8: $\mathbf{V}_{\text{conf}} \leftarrow$ list of $\mathcal{V}_{\text{conf}}$ sorted in decreasing $SD(v)$
- 9: **for** $v \in \mathbf{V}_{\text{conf}}$ **do**
- 10: $(C(v), \mathcal{C}_{\text{used}}) \leftarrow \text{COLORSELECT}(v, \mathcal{G}, C, \mathcal{C}_{\text{used}})$ in Algorithm 3
- 11: **end for**
- 12: **end if**
- 13: Recompute $\mathcal{V}_{\text{conf}}$
- 14: **if** $\mathcal{V}_{\text{conf}} = \emptyset$ **then**
- 15: **return** C
- 16: **end if**

Algorithm 3 Color Select

- 1: **function** COLORSELECT($v, \mathcal{G}, C, \mathcal{C}_{\text{used}}$)
- 2: $\mathcal{C}_{\mathcal{N}(v)} \leftarrow \{C(u) \mid u \in \mathcal{N}(v)\}$
- 3: First-fit strategy: select the minimum available color $c_{\text{new}} \leftarrow \min\{c \in \mathcal{C}_{\text{used}} \mid c \notin \mathcal{C}_{\mathcal{N}(v)}\}$
- 4: **if** c_{new} does not exist **then**
- 5: Add a new color $c_{\text{new}} \leftarrow \max(\mathcal{C}_{\text{used}}) + 1$
- 6: Update used colors $\mathcal{C}_{\text{used}} \leftarrow \mathcal{C}_{\text{used}} \cup \{c_{\text{new}}\}$
- 7: **end if**
- 8: **return** $(c_{\text{new}}, \mathcal{C}_{\text{used}})$
- 9: **end function**

vertices are ordered according to their indices, yielding the decreasing ordering list $\mathbf{V}_{\text{conf}} = (v_{1,3}, v_{2,1}, v_{3,2})$. The vertices in \mathbf{V}_{conf} are then recolored sequentially using Algorithm 3. The neighboring color sets of the conflicted vertices are

$$\mathcal{C}_{\mathcal{N}(v_{1,3})} = \{1, 2\}, \quad \mathcal{C}_{\mathcal{N}(v_{2,1})} = \{1, 2, 3\}, \quad \mathcal{C}_{\mathcal{N}(v_{3,2})} = \{1, 2, 3\}. \quad (27)$$

Following the first-fit strategy, vertex $v_{1,3}$ is assigned the minimum available color

$$c_{\text{new}} = \min\{c \in \mathcal{C}_{\text{used}} \mid c \notin \mathcal{C}_{\mathcal{N}(v_{1,3})}\} = \min\{c \in \{1, 2, 3\} \mid c \notin \{1, 2\}\} = 3. \quad (28)$$

After updating the color of $v_{1,3}$, the remaining conflicted vertices $v_{2,1}$ and $v_{3,2}$ are checked, and no further conflicts are detected in the graph. Consequently, a *proper coloring* is obtained as

$$C = \{C(v_{1,2}) = 1, C(v_{1,3}) = 3, C(v_{2,1}) = 1, C(v_{2,3}) = 2, C(v_{3,1}) = 3, C(v_{3,2}) = 2\}. \quad (29)$$

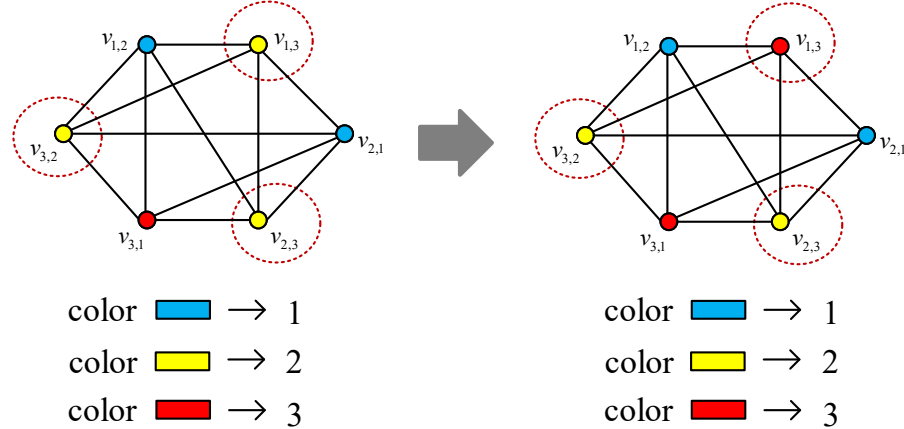


Fig. 7: The proposed postprocessing conflict repair procedure.

In summary, the proposed AI-aided framework for MACC systems with arbitrary user–cache topology combines a GNN-based coloring predictor with a postprocessing conflict repair mechanism. The GNN learns structural patterns to generate an initial coloring, and the conflict repair ensures a *proper coloring* with a small number of colors. This integration enables an efficient delivery phase and reduces the communication load in MACC systems.

V. LOW-COMPLEXITY CONVERSE BOUND BASED ON MACC-PDA

While the IC converse bound presented in Section III-C provides a theoretically tight characterization of the communication load, its computational complexity grows factorially with the number of users K , as it requires enumerating all possible user-demand permutations, i.e., $\mathcal{O}(K!)$. As K increases, this exhaustive enumeration quickly becomes computationally prohibitive, rendering the IC converse impractical for large-scale MACC systems. To address this limitation, we develop a low-complexity converse bound that exploits the structural properties of the MACC-PDA and adopts a greedy selection procedure. The proposed bound substantially reduces the computational burden while remaining highly accurate. In particular, it closely approximates the IC converse and, in many cases, exactly matches the optimal communication load.

The main idea is to exploit the structure of the MACC-PDA to avoid factorial enumeration of user demand permutations. Instead of exhaustively evaluating all permutations as in the IC converse, the method incrementally selects the column (user) whose demand set has the largest overlap with the currently accumulated set. This greedy accumulation of intersections yields an efficient approximation of the IC converse while requiring only linear operations per iteration.

The procedure can be summarized in three main steps:

- 1) **Extraction of user demand sets:** For each column of the user-retrieve array \mathbf{U} in the MACC-PDA (Definition 2), construct the set of uncached packets corresponding to the users' demands.
- 2) **Greedy accumulation of intersections:** Initialize an empty set and iteratively select a remaining column whose intersection with the current accumulated set is maximized.
- 3) **Approximate converse bound computation:** At each selection step, sum the sizes of the intersections obtained. According to (1), this cumulative sum directly corresponds to the communication load, providing a tight approximation without enumerating all column permutations.

To further illustrate the operation of the greedy converse algorithm, we present a small example based on the MACC-PDA in Example 1. The column selection process and the resulting approximate communication load are summarized in Table I.

Example 4. We consider the 6×4 user-retrieve array \mathbf{U} of MACC-PDA in Example 1, as shown in Fig. 8, where each row indicates whether the corresponding packet is uncached or requested.

Algorithm 4 Greedy converse algorithm based on MACC-PDA

```

1: Input: User-retrieve array  $\mathbf{U}$  of MACC-PDA
2: Output: Transmission load  $R$ 
3: Initialize accumulated set  $\mathcal{S} \leftarrow \emptyset$ , cumulative sum  $S \leftarrow 0$ , remaining columns  $\mathcal{K}_{\text{remain}} \leftarrow [K]$ ,
   user demand set  $\mathcal{S}_{d_k}, k \in [K]$ 
4: while  $\mathcal{K}_{\text{remain}} \neq \emptyset$  do
5:   for each column  $k \in \mathcal{K}_{\text{remain}}$  do
6:     if  $\mathcal{S} \neq \emptyset$  then
7:       Compute intersection  $\mathcal{I}_k \leftarrow \mathcal{S} \cap \mathcal{S}_{d_k}$ 
8:     else
9:        $\mathcal{I}_k \leftarrow \mathcal{S}_{d_k}$ 
10:    end if
11:   end for
12:   Select column  $k' \leftarrow \arg \max_{k \in \mathcal{K}_{\text{remain}}} |\mathcal{I}_k|$ 
13:   Update accumulated set  $\mathcal{S} \leftarrow \mathcal{I}_{k'}$ , cumulative sum  $S \leftarrow S + |\mathcal{S}|$ 
14:   Remove  $k'$  from  $\mathcal{K}_{\text{remain}}$ 
15: end while
16: return  $R = \frac{S}{F}$ 
  
```

Initially, the remaining column set is $\mathcal{K}_{\text{remain}} = \{1, 2, 3, 4, 5\}$, the accumulated set is $\mathcal{S} = \emptyset$, and the cumulative load is $S = 0$. The sets of uncached or requested packets associated with each user k are given by

$$\mathcal{S}_{d_1} = \{6\}, \mathcal{S}_{d_2} = \{5\}, \mathcal{S}_{d_3} = \{1, 2, 4\}, \mathcal{S}_{d_4} = \{2, 3, 5\}, \mathcal{S}_{d_5} = \{1, 3, 5\}. \quad (30)$$

By Lines 4-11 of Algorithm 4, we compute the intersection $\mathcal{I}_k = \mathcal{S} \cap \mathcal{S}_{d_k}$ for each $k \in \mathcal{K}_{\text{remain}} = \{1, 2, 3, 4, 5\}$. Since the accumulated set is initially empty, i.e., $\mathcal{S} = \emptyset$, it follows that

$$\mathcal{I}_k = \mathcal{S}_{d_k}, k = 1, 2, 3, 4, 5. \quad (31)$$

The corresponding cardinalities are

$$|\mathcal{I}_1| = |\mathcal{I}_2| = 1, \quad |\mathcal{I}_3| = |\mathcal{I}_4| = |\mathcal{I}_5| = 3. \quad (32)$$

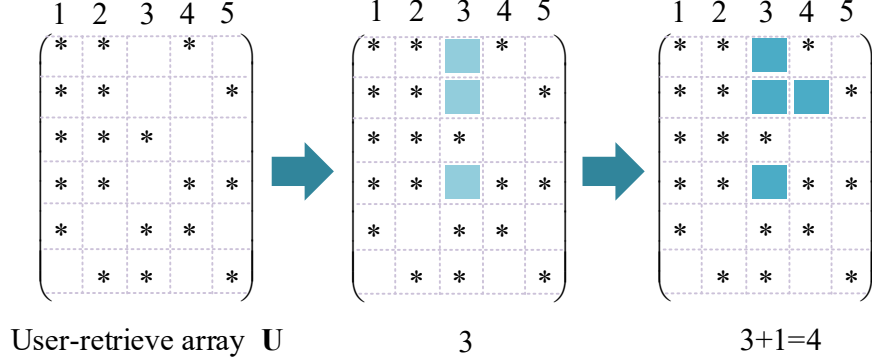


Fig. 8: The procedure of greedy converse.

Consequently, Line 12 selects a column with the largest intersection cardinality. Among columns 3, 4, 5, which all attain the maximum value, we arbitrarily select $k' = 3$. Following Lines 13–15, the accumulated set is updated to $\mathcal{S} = \mathcal{I}_3$, the cumulative sum becomes $S = |\mathcal{S}| = 3$, and column 3 is removed from $\mathcal{K}_{\text{remain}}$. This greedy selection procedure is repeated until all columns have been processed. The detailed operations at each iteration are listed in Table I. After the final iteration, Line 17 returns the greedy converse bound $R = \frac{S}{F} = \frac{4}{6} = \frac{2}{3}$.

TABLE I: Selection process for example 4

Chosen	$\mathcal{K}_{\text{remain}}$	\mathcal{I}_k	k'	$(\mathcal{S}, \mathcal{S} , R)$
1	$\{1, 2, 3, 4, 5\}$	$\mathcal{I}_1 = \{6\}$ $\mathcal{I}_2 = \{5\}$ $\mathcal{I}_3 = \{1, 2, 4\}$ $\mathcal{I}_4 = \{2, 3, 5\}$ $\mathcal{I}_5 = \{1, 3, 5\}$	$k' = 3$	$\mathcal{S} = \mathcal{I}_3, \mathcal{S} = 3, R = 3$
2	$\{1, 2, 4, 5\}$	$\mathcal{I}_1 = \mathcal{S} \cap \mathcal{S}_{d_1} = \emptyset$ $\mathcal{I}_2 = \mathcal{S} \cap \mathcal{S}_{d_2} = \emptyset$ $\mathcal{I}_4 = \mathcal{S} \cap \mathcal{S}_{d_4} = \{2\}$ $\mathcal{I}_5 = \mathcal{S} \cap \mathcal{S}_{d_5} = \{1\}$	$k' = 4$	$\mathcal{S} = \mathcal{I}_4, \mathcal{S} = 1, S = 3 + 1 = 4$
3	$\{1, 2, 5\}$	$\mathcal{I}_1 = \mathcal{S} \cap \mathcal{S}_{d_1} = \emptyset$ $\mathcal{I}_2 = \mathcal{S} \cap \mathcal{S}_{d_2} = \emptyset$ $\mathcal{I}_5 = \mathcal{S} \cap \mathcal{S}_{d_5} = \emptyset$	$k' = 1$	$\mathcal{S} = \mathcal{I}_1, \mathcal{S} = 0, S = 4$
4	$\{2, 5\}$	$\mathcal{I}_2 = \mathcal{S} \cap \mathcal{S}_{d_2} = \emptyset$ $\mathcal{I}_5 = \mathcal{S} \cap \mathcal{S}_{d_5} = \emptyset$	$k' = 2$	$\mathcal{S} = \mathcal{I}_2, \mathcal{S} = 0, S = 4$
5	$\{5\}$	$\mathcal{I}_5 = \mathcal{S} \cap \mathcal{S}_{d_5} = \emptyset$	-	$\mathcal{S} = \mathcal{I}_5, \mathcal{S} = 0, S = 4$

Finally, we compare the proposed greedy converse bound with the IC converse in Section III-C for the user-retrieve array \mathbf{U} under consideration. The IC converse requires evaluating all permutations of the 5 user requests, resulting in $5! = 120$ possible orderings. According to (12), the IC converse bound is given by

$$\begin{aligned} R &\geq \max_{\mathbf{u} \in \mathfrak{U}} R_{\mathbf{u}} = \max_{\mathbf{u} \in \mathfrak{U}} \sum_{i \in [K]} \sum_{\mathcal{J}_{u_i} \subseteq [\Lambda] \setminus \bigcup_{j=1}^i \mathcal{A}_{u_j}} \frac{|W_{d_{u_i}, \mathcal{J}_{u_i}}|}{F} \\ &= \max_{\mathbf{u} \in \mathfrak{U}} \sum_{i=1}^5 \sum_{\mathcal{J}_{u_i} \subseteq [\Lambda] \setminus \bigcup_{j=1}^i \mathcal{A}_{u_j}} \frac{|W_{d_{u_i}, \mathcal{J}_{u_i}}|}{6}, \end{aligned} \quad (33)$$

where $|W_{d_{u_i}, \mathcal{J}_{u_i}}|$ denotes the number of packets of file $W_{d_{u_i}}$ that are not available at the cache nodes indexed by $\bigcup_{j=1}^i \mathcal{A}_{u_j}$. Among all user permutations, consider $\mathbf{u} = (3, 4, 1, 2, 5)$, which achieves the maximum load. The corresponding IC converse sum is

$$\begin{aligned} R_{\mathbf{u}} &= \frac{1}{6} \left(|\mathcal{S}_{d_3}| + |\mathcal{S}_{d_4} \cap \mathcal{S}_{d_3}| + |\mathcal{S}_{d_1} \cap \mathcal{S}_{d_4}| + |\mathcal{S}_{d_2} \cap \mathcal{S}_{d_1}| + |\mathcal{S}_{d_5} \cap \mathcal{S}_{d_2}| \right) \\ &= \frac{1}{6} (3 + 1 + 0 + 0 + 0) = \frac{2}{3}. \end{aligned} \quad (34)$$

Notably, this value exactly coincides with the greedy converse load obtained in Example 4. In contrast to the IC converse, which requires evaluating all 120 permutations, the greedy approach only computes the intersections for the remaining columns at each iteration. As a result, the total number of intersection computations is reduced to $5 + 4 + 3 + 2 + 1 = 15$, demonstrating a substantial reduction in computational complexity while achieving the same converse bound in this example.

For a system with K users, the IC converse requires $\mathcal{O}(K!)$ operations, which quickly becomes computationally intractable as K increases. In contrast, the proposed greedy converse involves only K sequential greedy selections. At each iteration, the algorithm computes intersections over the remaining users, resulting in an overall complexity of $\mathcal{O}(K^2)$. This represents a dramatic reduction from factorial to polynomial complexity, making the greedy converse scalable for large-scale MACC-PDA systems.

As demonstrated in Example 4, the greedy converse exactly matches the optimal IC converse for the MN PDA. This exactness stems from the strong structural regularity inherent in MN PDAs. Specifically, in an MN PDA, each column contains the same number of stars, and the star locations follow a highly symmetric combinatorial design, each row corresponds to one subset in

$\binom{[K]}{t}$, and every such subset appears exactly once. As a result, the request sets of all users have identical cardinalities and exhibit uniform intersection patterns for any pair of users. Owing to this symmetry, all columns are effectively interchangeable at the beginning of the greedy procedure. Consequently, at each iteration, the greedy selection always achieves the maximum possible intersection size, which guarantees that the greedy converse attains the optimal load for all MN PDAs. For general MACC-PDA structures, where the user–cache access topology is arbitrary, the star patterns in the user-retrieve array \mathbf{U} are no longer uniform. Nevertheless, the greedy converse continues to provide a tight approximation by prioritizing, at each iteration, the user whose demand set contributes the most to the accumulated intersection. Although the intersection sizes are not uniform in this case, the early selections typically dominate the overall load, resulting in a converse value that is very close to the optimal IC bound. Extensive numerical results in Section VI confirm that the greedy converse consistently yields near-optimal performance even for large-scale and highly irregular MACC-PDA instances, while significantly reducing computational complexity.

VI. EXPERIMENTS

In this section, we evaluate the performance of the proposed AI-aided framework for MACC systems with arbitrary cache–user access topology. The evaluation focuses on two aspects, (i) the effectiveness of the proposed GNN-based approach in constructing efficient delivery schemes, and (ii) the tightness and computational efficiency of the proposed greedy converse bound. Through extensive simulations, we compare the proposed methods with conventional schemes in terms of delivery load and computational complexity under a variety of user–cache access configurations.

A. Experimental setup

We consider a MACC system consisting of K user nodes and Λ cache nodes. Each user node is connected to a subset of cache nodes according to a user–cache access topology $\mathcal{A} = \{\mathcal{A}_k \mid k \in [K]\}$. The access topology are randomly generated under the following constraints:

- a) Each user node is connected to at least one cache node;
- b) Each cache node is accessed by at least one user node.

User–cache connections are constructed via a randomized procedure that enforces the above constraints while allowing heterogeneous user degrees. Consequently, the resulting access topology

are irregular and diverse, capturing practical MACC scenarios with arbitrary and non-uniform cache–user access patterns.

Simulation setup: The proposed framework is compared with the following coded caching schemes and converse bounds.

- *Graph coloring approaches*

- GNN-based approach: The proposed learning-based delivery design described in Section IV.
- DSatur: The classical DSatur heuristic graph coloring algorithm applied to the conflict graph, serving as a strong non-learning baseline in Section III-A.
- GIN-based approach [47]: A graph coloring approach based on Graph Isomorphism Networks.

- *Converse bounds*

- IC converse: The optimal converse bound on the transmission load derived in Section III-C.
- Greedy converse: The proposed low-complexity greedy approximation to the IC converse presented in Section V.

Evaluation metrics: The primary performance metric is the *transmission load*, defined as the number of transmissions normalized by the subpacketization level. After the postprocessing stage, this metric is equivalently characterized by the number of colors used in the final graph coloring, which directly corresponds to the number of transmissions in the delivery phase.

Implementation details: The GNN models are implemented using PyTorch Geometric and trained following the procedure described in Section IV. All experiments are conducted on a workstation equipped with a GPU. The reported results are averaged over multiple randomly generated access topology to ensure statistical robustness. The detailed training configurations are summarized in Table II.

B. Performance of the graph coloring approaches

We evaluate the performance of the proposed learning-based graph coloring framework for constructing the delivery phase in MACC systems. For each user number K and cache node number Λ , 50 independent user–cache access topology are generated, and all results are averaged to ensure statistical robustness. The transmission load is quantified by the number of colors

TABLE II: GNN training configuration

Parameter	Value
Number of users K	4-20
Number of cache nodes Λ	10
Topologies per K	1500
User degree	1-10
Number of GCN layers	3
Hidden dimension d	128
Optimizer	AdamW
Learning rate η	1×10^{-4}
Batch size	32
Training epochs	2000
Softmax temperature τ	1.0
Potts loss weight J	1
Color-count regularization β	0.1

obtained after the postprocessing stage, which directly corresponds to the number of multicast transmissions (parameter S in Definition 1). We first adopt the classical DSatur graph coloring in Algorithm 1 as a non-learning baseline and compare its performance with the theoretical IC converse bound. Fig. 9 illustrates the variation of the color ratio $S_{\text{DSatur}}/S_{\text{IC}}$ with respect to the user number K when the cache node number is fixed to $\Lambda = 10$. It can be observed that, across different user scales, the transmission load achieved by DSatur remains very close to the IC converse bound, with a maximum gap no greater than 1.2%. This result indicates that DSatur achieves near-optimal performance in the MACC setting and therefore serves as a reliable and competitive benchmark for evaluating learning-based graph coloring approaches. On this basis, we further assess the performance of the proposed GNN model in the delivery phase of the MACC system.

Performance evaluation of the GNN model: To comprehensively evaluate the effectiveness of the proposed GNN model, we performed experimental analysis from both perspective of computational efficiency and transmission load. Unless otherwise specified, all experiments are performed with the number of user nodes $K \in \{6, 8, 10, 13, 16, 19\}$ and a fixed number of cache nodes $\Lambda = 10$.

a) Performance evaluation under a fixed number of user nodes: When the number of user nodes in the testing phase is identical to that used during training, Figs. 10a and 10b compare the proposed GNN-based approach with the GIN-based approach in [47] in terms

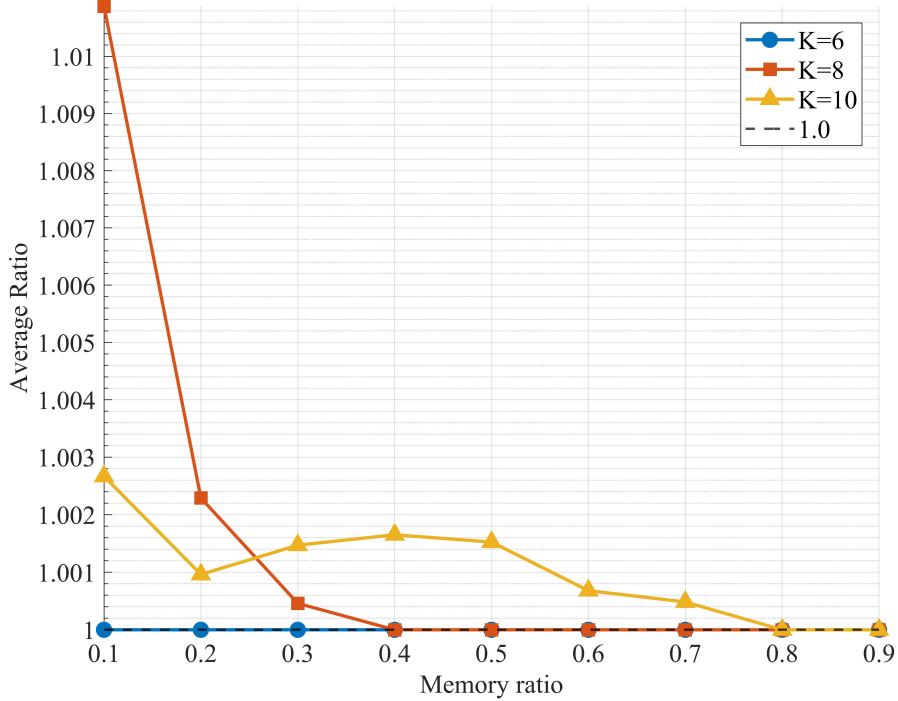


Fig. 9: Ratio between the number of colors produced by DSatur in Algorithm 1 and the IC converse bound.

of the runtime ratio $T_{\text{DSatur}}/T_{\text{GNN}}$ and the color ratio $S_{\text{DSatur}}/S_{\text{GNN}}$, respectively. The results indicate that the proposed GNN-based approach substantially reduces computational complexity while maintaining a transmission load close to that of DSatur. As the number of users increases, the GNN achieves a runtime reduction by a factor ranging from approximately 20-30 compared with DSatur, while the number of required colors remains consistently within 10% of the DSatur solution. When the number of user nodes is smaller than 10 and the cache ratio is relatively high, this gap further decreases to within 5%.

Compared with the GIN-based, as illustrated in Figs. 10c and 10d, the proposed GNN demonstrates a significantly higher computational efficiency, achieving runtime reductions on the order of one to two orders of magnitude. Moreover, GIN-based approach requires a larger number of colors than the proposed GNN, approximately 70%-80% under low cache ratios and 30%-60% under moderate cache ratios. Only when the cache ratio approaches 0.9 and the graph size becomes small do the runtimes of the two approaches become comparable.

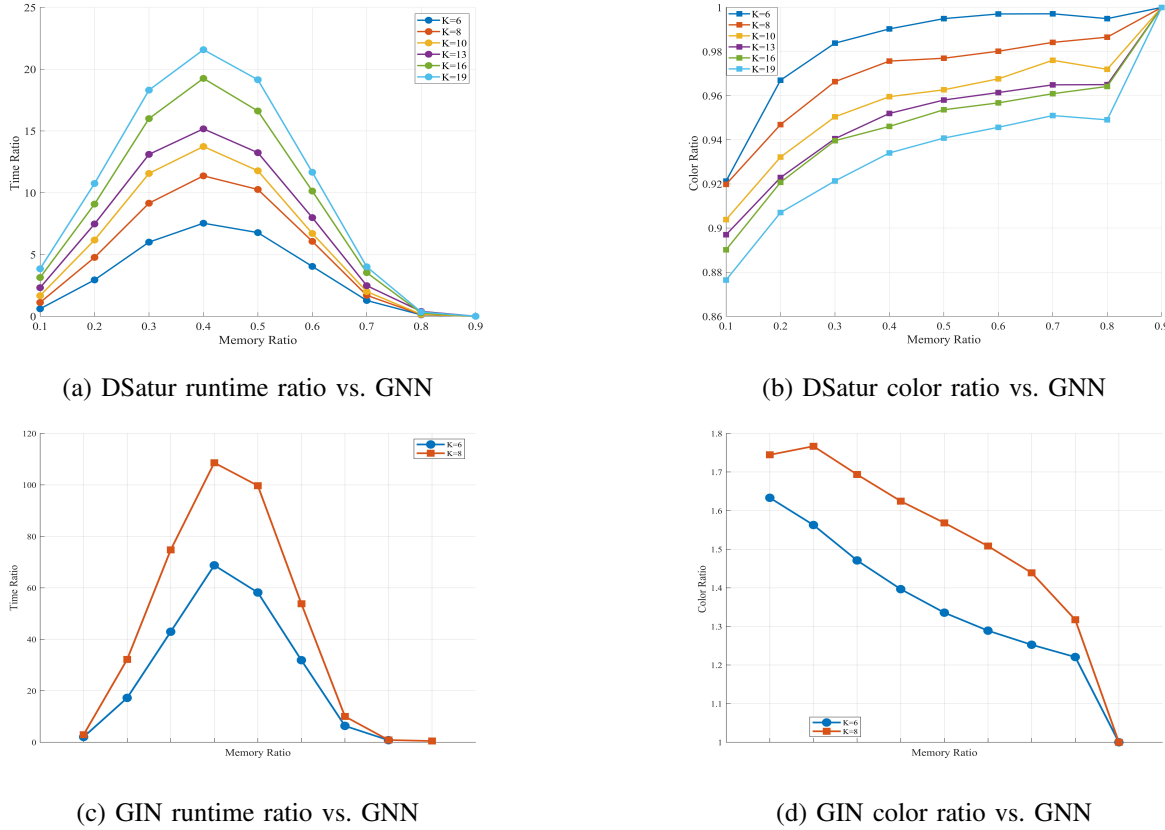


Fig. 10: Performance comparison of the proposed GNN-based approach and the GIN-based approach [47] for fixed numbers of user nodes.

b) Generalization performance under varying user numbers: To evaluate the generalization capability of the proposed GNN-based approach across different number of user nodes, we train a single model in which the number of user nodes during training is uniformly sampled from the interval $K \in [4, 20]$. After training, this model is directly applied to MACC systems with user numbers $K \in \{6, 8, 10, 13, 16, 19\}$. Figs. 11a and 11b depict the runtime ratio $T_{\text{DSatur}}/T_{\text{GNN}}$ and the color ratio $S_{\text{DSatur}}/S_{\text{GNN}}$, respectively. It can be observed that, as the number of users increases, the computational advantage of the GNN over DSatur becomes increasingly pronounced, while the achieved transmission load consistently remains close to that of DSatur. This behavior is consistent with the results obtained under fixed user numbers and demonstrates that the proposed GNN framework generalizes well across different number of user and access topology, making it suitable for practical MACC systems.

Remark 2. For each system configuration, all reported results are averaged over 50 independently

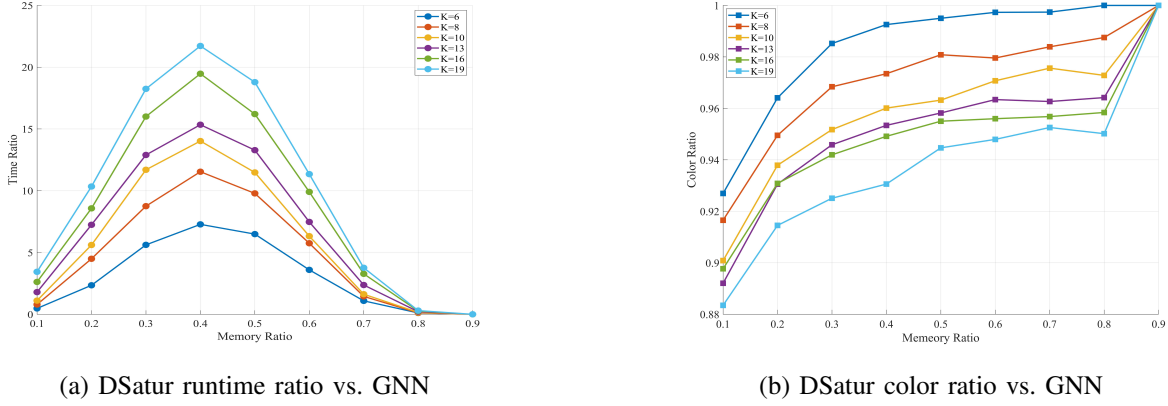


Fig. 11: Performance of the proposed GNN-based approach across varying numbers of user nodes.

generated user–cache access topology with random user demands. The DSatur algorithm serves as a strong non-learning benchmark, whose performance is very close to the IC converse bound. As shown in Figs. 11a, 11b, 10c and 10d, the proposed GNN-based approach consistently achieves delivery loads that closely match those of DSatur, while substantially reducing the computational runtime. Moreover, the observed performance trends remain highly consistent across different training and testing settings, including scenarios where the GNN is trained and evaluated on a fixed number of user nodes, as well as scenarios where it is trained over a mixture of user numbers and tested on a specific K . These results suggest that the learned coloring policy captures fundamental structural characteristics of MACC conflict graphs that are shared across different system configurations, rather than overfitting to a particular topology or user population. Consequently, the proposed framework exhibits strong robustness and transferability, making it well suited for practical MACC systems with dynamically varying numbers of users and access topology.

C. Greedy converse bound and computational efficiency

We next evaluate the proposed greedy converse bound, which serves as a low-complexity approximation to the IC converse. The evaluation focuses on both the tightness of the greedy bound relative to the IC converse and its computational efficiency. Fig. 12a compares the greedy converse with the IC converse for varying numbers of user nodes K , with the number of cache nodes fixed at $\Lambda = 10$. As shown in the figure, the greedy bound consistently remains close to the IC converse, and the approximation gap remains nearly unchanged as the number of users

increases. This indicates that the accuracy of the greedy approximation does not deteriorate with system scale. Fig. 12b illustrates the corresponding runtime comparison. The greedy converse achieves orders-of-magnitude reductions in computation time compared to the IC converse. Moreover, the computational advantage becomes increasingly pronounced as the number of user nodes grows, highlighting the scalability of the proposed greedy approach.

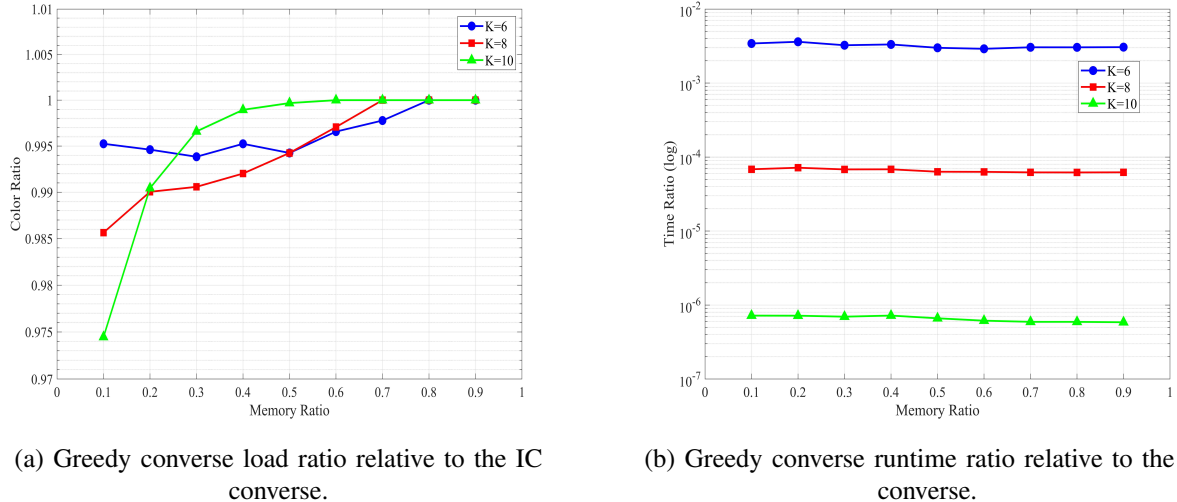


Fig. 12: Performance comparison between the proposed greedy converse and the IC converse for different numbers of users.

To further quantify this observation, Table III reports detailed numerical results for a representative system with $K = 10$ users and $\Lambda = 10$ cache nodes. The table shows that the greedy converse achieves more than 97% of the IC converse load across all cache memory ratios, while offering dramatic reductions in computation time, approximately 10^{-2} , 10^{-4} , and 10^{-6} of the IC converse runtime for $K = 6$, 8, and 10, respectively. In several cases, the greedy bound matches the IC converse exactly. These results demonstrate that the proposed greedy converse provides an accurate and computationally efficient alternative to the IC converse for MACC systems with arbitrary access topology.

VII. CONCLUSION

This paper investigated MACC systems with arbitrary user–cache access topology. Focusing on the delivery phase under a fixed cache placement, we first proposed a universal graph-based formulation that transforms the delivery problem into a graph coloring problem. Within this framework, the classical DSatur algorithm was shown to achieve delivery loads close to the

TABLE III: Comparison between the greedy converse and the IC converse for $K = 10$ users and $\Lambda = 10$ cache nodes.

Cache memory ratio	Load ratio $\left(\frac{S_{\text{greedy}}}{S_{\text{IC}}} \times 100\%\right)$	Runtime ratio $\left(\frac{T_{\text{greedy}}}{T_{\text{IC}}}\right)$
1/10	97.446%	7.200×10^{-7}
2/10	99.044%	7.182×10^{-7}
3/10	99.659%	6.966×10^{-7}
4/10	99.894%	7.209×10^{-7}
5/10	99.968%	6.624×10^{-7}
6/10	100.000%	6.149×10^{-7}
7/10	100.000%	5.933×10^{-7}
8/10	100.000%	5.930×10^{-7}
9/10	100.000%	5.857×10^{-7}

IC converse bound, serving as a strong and practical performance benchmark. To address the computational challenges associated with large-scale graphs, we further developed a GNN-based graph coloring framework that learns efficient coloring policies directly from graph structures. The proposed learning-based approach achieves delivery loads comparable to DSatur while substantially reducing computational time, and exhibits strong generalization across diverse access topology and varying numbers of users. In addition, we extended the IC converse to MACC systems with arbitrary access structures and proposed a low-complexity greedy approximation. The greedy converse was shown to closely match the IC converse while offering orders-of-magnitude reductions in computational complexity. Future work may consider joint optimization of cache placement and delivery strategies, as well as extensions to dynamic or time-varying user–cache access topology.

REFERENCES

- [1] G. S. Paschos, G. Iosifidis, M. Tao, D. Towsley, and G. Caire, “The role of caching in future communication systems and networks,” *IEEE Journal on Selected Areas in Communications*, vol. 36, no. 6, pp. 1111–1125, 2018.
- [2] M. A. Maddah-Ali and U. Niesen, “Fundamental limits of caching,” *IEEE Transactions on information theory*, vol. 60, no. 5, pp. 2856–2867, 2014.
- [3] K. Wan, D. Tuninetti, and P. Piantanida, “An index coding approach to caching with uncoded cache placement,” *IEEE Transactions on Information Theory*, vol. 66, no. 3, pp. 1318–1332, 2020.
- [4] Q. Yan, M. Cheng, X. Tang, and Q. Chen, “On the placement delivery array design for centralized coded caching scheme,” *IEEE Transactions on Information Theory*, vol. 63, no. 9, pp. 5821–5833, 2017.
- [5] M. Cheng, J. Wang, X. Zhong, and Q. Wang, “A framework of constructing placement delivery arrays for centralized coded caching,” *IEEE Transactions on Information Theory*, vol. 67, no. 11, pp. 7121–7131, 2021.

- [6] J. Wang, M. Cheng, K. Wan, and G. Caire, "Placement delivery array construction via cartesian product for coded caching," *IEEE Transactions on Information Theory*, vol. 69, no. 12, pp. 7602–7626, 2023.
- [7] —, "A framework of constructing pda via union of cache configurations from cartesian product," in *2025 IEEE International Symposium on Information Theory (ISIT)*. IEEE, 2025, pp. 1–6.
- [8] H. Wei, M. Cheng, and K. Leung, "A novel construction of coded caching schemes with polynomial subpacketizations via projective geometry," in *2024 IEEE Information Theory Workshop (ITW)*. IEEE, 2024, pp. 496–501.
- [9] M. Cheng, Y. Li, X. Zhong, and R. Wei, "Improved constructions of coded caching schemes for combination networks," *IEEE Transactions on Communications*, vol. 68, no. 10, pp. 5965–5975, 2020.
- [10] M. Ji, G. Caire, and A. F. Molisch, "Fundamental limits of caching in wireless d2d networks," *IEEE Transactions on Information Theory*, vol. 62, no. 2, pp. 849–869, 2015.
- [11] Y. Kong, Y. Wu, and M. Cheng, "Combinatorial designs for coded caching on hierarchical networks," in *2023 IEEE Wireless Communications and Networking Conference (WCNC)*. IEEE, 2023, pp. 1–6.
- [12] T. Yang, K. Wan, M. Cheng, R. C. Qiu, and G. Caire, "Multiple-antenna placement delivery array for cache-aided miso systems," *IEEE Transactions on Information Theory*, 2023.
- [13] E. Lampiris and P. Elia, "Adding transmitters dramatically boosts coded-caching gains for finite file sizes," *IEEE Journal on Selected Areas in Communications*, vol. 36, no. 6, pp. 1176–1188, 2018.
- [14] N. Naderializadeh, M. A. Maddah-Ali, and A. S. Avestimehr, "Fundamental limits of cache-aided interference management," *IEEE Transactions on Information Theory*, vol. 63, no. 5, pp. 3092–3107, 2017.
- [15] K. K. Namboodiri, E. Peter, and B. S. Rajan, "Extended placement delivery arrays for multi-antenna coded caching scheme," *IEEE Transactions on Communications*, 2023.
- [16] M. Salehi, E. Parrinello, S. P. Shariatpanahi, P. Elia, and A. Tölli, "Low-complexity high-performance cyclic caching for large miso systems," *IEEE Transactions on Wireless Communications*, vol. 21, no. 5, pp. 3263–3278, 2021.
- [17] X. Niu, M. Cheng, K. Wan, R. C. Qiu, and G. Caire, "Reflecting intelligent surfaces-assisted multiple-antenna coded caching," in *2024 IEEE Information Theory Workshop (ITW)*. IEEE, 2024, pp. 490–495.
- [18] M. Cheng, K. Wan, D. Liang, M. Zhang, and G. Caire, "A novel transformation approach of shared-link coded caching schemes for multiaccess networks," *IEEE Transactions on Communications*, vol. 69, no. 11, pp. 7376–7389, 2021.
- [19] S. Sasi and B. S. Rajan, "Multi-access coded caching scheme with linear sub-packetization using pdas," *IEEE Transactions on Communications*, vol. 69, no. 12, pp. 7974–7985, 2021.
- [20] J. Wang, M. Cheng, Y. Wu, and X. Li, "Multi-access coded caching with optimal rate and linear subpacketization under pda and consecutive cyclic placement," *IEEE Transactions on Communications*, vol. 71, no. 6, pp. 3178–3190, 2023.
- [21] M. Zhang, K. Wan, M. Cheng, and G. Caire, "Coded caching for two-dimensional multi-access networks," in *2022 IEEE International Symposium on Information Theory (ISIT)*. IEEE, 2022, pp. 1707–1712.
- [22] J. Hachem, N. Karamchandani, and S. N. Diggavi, "Coded caching for multi-level popularity and access," *IEEE Transactions on Information Theory*, vol. 63, no. 5, pp. 3108–3141, 2017.
- [23] K. S. Reddy and N. Karamchandani, "Structured index coding problem and multi-access coded caching," *IEEE Journal on Selected Areas in Information Theory*, vol. 2, no. 4, pp. 1266–1281, 2021.
- [24] F. Brunero and P. Elia, "Fundamental limits of combinatorial multi-access caching," *IEEE Transactions on Information Theory*, vol. 69, no. 2, pp. 1037–1056, 2022.
- [25] K. K. Namboodiri and B. S. Rajan, "Combinatorial multi-access coded caching: Improved rate-memory trade-off with coded placement," *IEEE Transactions on Information Theory*, vol. 70, no. 3, pp. 1787–1805, 2024.
- [26] D. Katyal, P. N. Muralidhar, and B. S. Rajan, "Multi-access coded caching schemes from cross resolvable designs," *IEEE Transactions on Communications*, vol. 69, no. 5, pp. 2997–3010, 2021.

- [27] N. Das and B. S. Rajan, "Multi-access coded caching schemes from maximal cross resolvable designs," in *2022 IEEE International Symposium on Information Theory (ISIT)*. IEEE, 2022, pp. 1719–1724.
- [28] P. N. Muralidhar and B. S. Rajan, "Multi-access coded caching from a new class of cross resolvable designs," in *2021 IEEE International Symposium on Information Theory (ISIT)*. IEEE, 2021, pp. 855–860.
- [29] M. Cheng, K. Wan, P. Elia, and G. Caire, "Coded caching schemes for multiaccess topologies via combinatorial design," *IEEE Transactions on Information Theory*, 2025.
- [30] Z. Zhang and M. Tao, "Deep learning for wireless coded caching with unknown and time-variant content popularity," *IEEE Transactions on Wireless Communications*, vol. 20, no. 2, pp. 1152–1163, 2020.
- [31] Y. Zhou, M. Peng, S. Yan, and Y. Sun, "Deep reinforcement learning based coded caching scheme in fog radio access networks," in *2018 IEEE/CIC International Conference on Communications in China (ICCC Workshops)*. IEEE, 2018, pp. 309–313.
- [32] A. Sengupta, S. Amuru, R. Tandon, R. M. Buehrer, and T. C. Clancy, "Learning distributed caching strategies in small cell networks," in *2014 11th International Symposium on Wireless Communications Systems (ISWCS)*. IEEE, 2014, pp. 917–921.
- [33] X. Wu, J. Li, M. Xiao, P. Ching, and H. V. Poor, "Multi-agent reinforcement learning for cooperative coded caching via homotopy optimization," *IEEE Transactions on Wireless Communications*, vol. 20, no. 8, pp. 5258–5272, 2021.
- [34] S. Gao, P. Dong, Z. Pan, and G. Y. Li, "Reinforcement learning based cooperative coded caching under dynamic popularities in ultra-dense networks," *IEEE Transactions on Vehicular Technology*, vol. 69, no. 5, pp. 5442–5456, 2020.
- [35] J. Song, M. Sheng, T. Q. Quek, C. Xu, and X. Wang, "Learning-based content caching and sharing for wireless networks," *IEEE Transactions on Communications*, vol. 65, no. 10, pp. 4309–4324, 2017.
- [36] Z. Zhang, H. Chen, M. Hua, C. Li, Y. Huang, and L. Yang, "Double coded caching in ultra dense networks: Caching and multicast scheduling via deep reinforcement learning," *IEEE Transactions on Communications*, vol. 68, no. 2, pp. 1071–1086, 2019.
- [37] N. Naderizadeh and S. M. Asghari, "Learning to code: Coded caching via deep reinforcement learning," in *2019 53rd Asilomar Conference on Signals, Systems, and Computers*. IEEE, 2019, pp. 1774–1778.
- [38] Z. Shan, X. Yi, H. Yu, C.-S. Liao, and S. Jin, "Revisiting topological interference management: A learning-to-code on graphs perspective," *arXiv preprint arXiv:2502.09344*, 2025.
- [39] J. A. Bondy, U. S. R. Murty *et al.*, *Graph theory with applications*. Macmillan London, 1976, vol. 290.
- [40] J. Hartmanis, "Computers and intractability: a guide to the theory of np-completeness (michael r. garey and david s. johnson)," *Siam Review*, vol. 24, no. 1, p. 90, 1982.
- [41] P. N. Muralidhar, D. Katyal, and B. S. Rajan, "Maddah-ali-niesen scheme for multi-access coded caching," in *2021 IEEE Information Theory Workshop (ITW)*. IEEE, 2021, pp. 1–6.
- [42] K. S. Reddy and N. Karamchandani, "Rate-memory trade-off for multi-access coded caching with uncoded placement," *IEEE Transactions on Communications*, vol. 68, no. 6, pp. 3261–3274, 2020.
- [43] D. Brélaz, "New methods to color the vertices of a graph," *Communications of the ACM*, vol. 22, no. 4, pp. 251–256, 1979.
- [44] O. Goudet, C. Grelier, and J.-K. Hao, "A deep learning guided memetic framework for graph coloring problems," *Knowledge-Based Systems*, vol. 258, p. 109986, 2022.
- [45] W. Li, R. Li, Y. Ma, S. O. Chan, and B. Yu, "Rethinking graph neural networks for graph coloring," 2020.
- [46] M. J. Schuetz, J. K. Brubaker, Z. Zhu, and H. G. Katzgraber, "Graph coloring with physics-inspired graph neural networks," *Physical Review Research*, vol. 4, no. 4, p. 043131, 2022.

- [47] Y. Zhang, K. Zhang, and N. Wu, “Using graph isomorphism network to solve graph coloring problem,” in *2024 4th International Conference on Consumer Electronics and Computer Engineering (ICCECE)*. IEEE, 2024, pp. 209–215.
- [48] F.-Y. Wu, “The potts model,” *Reviews of modern physics*, vol. 54, no. 1, p. 235, 1982.
- [49] T. Kipf, “Semi-supervised classification with graph convolutional networks,” *arXiv preprint arXiv:1609.02907*, 2016.
- [50] A. Hertz and D. de Werra, “Using tabu search techniques for graph coloring,” *Computing*, vol. 39, no. 4, pp. 345–351, 1987.
- [51] W. Li, R. Li, Y. Ma, S. O. Chan, D. Pan, and B. Yu, “Rethinking graph neural networks for the graph coloring problem,” *arXiv preprint arXiv:2208.06975*, 2022.
- [52] M. Gao and J. Hu, “Graph coloring algorithm based on minimal cost graph neural network,” *IEEE Access*, 2024.
- [53] A. Z. Ijaz, R. H. Ali, N. Ali, T. Laique, and T. A. Khan, “Solving graph coloring problem via graph neural network (gnn),” in *2022 17th International Conference on Emerging Technologies (ICET)*. IEEE, 2022, pp. 178–183.
- [54] F. Arbabjolfaei, B. Bandemer, Y.-H. Kim, E. Şaşoğlu, and L. Wang, “On the capacity region for index coding,” in *2013 IEEE International Symposium on Information Theory*. IEEE, 2013, pp. 962–966.